AD-A116 118 ARMY ELECTRONICS RESEARCH AND DEVELOPMENT COMMAND WS--ETC F/G 1/3
THE MANEUVERABLE ATMOSPHERIC PROBE (MAP), A REMOTELY PILOTED VE--ETC(U)
MAY 82 R RUBIO, C L TATE, M L HILL

UNCLASSIFIED ERADCOM/ASL-TR-0110 NL

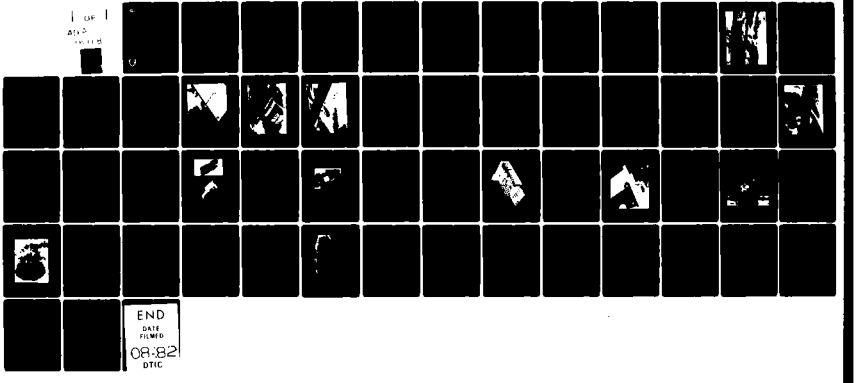

END
DATE FILMED
08-82
DTIC

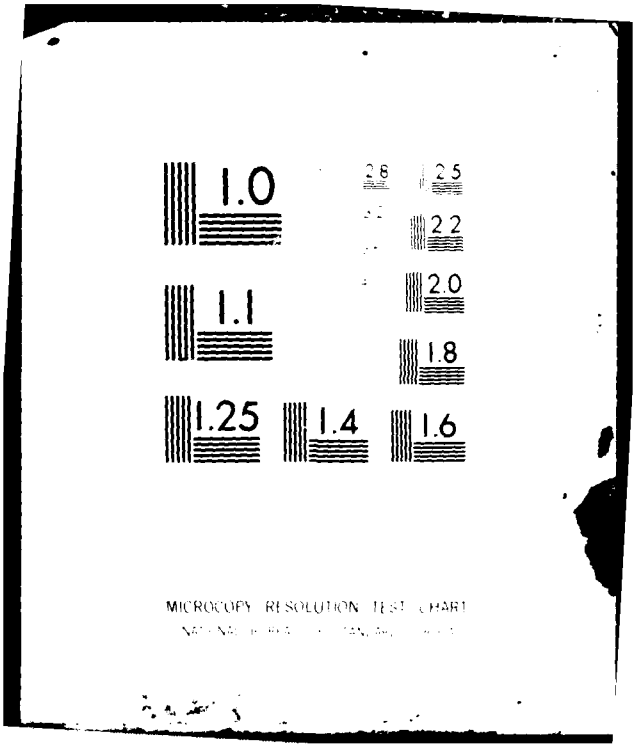
1.0
2.8
2.5
2.2
1.1
2.0
1.8
1.25
1.4
1.6
MICROCOPY RESOLUTION TEST CHART

TR-0110

AD

Reports Control Symbol
OSD - 1366

THE MANEUVERABLE ATMOSPHERIC PROBE (MAP), A REMOTELY PILOTED VEHICLE

MAY 1982

By

Roberto Rubio
Claude L. Tate

US Army Atmospheric Sciences Laboratory
White Sands Missile Range, NM

Maynard L. Hill

Applied Physics Laboratory
Johns Hopkins University
Baltimore, MD

Harold N. Ballard
Mike Izquierdo
Carlos McDonald

Electrical Engineering Department
The University of Texas at El Paso
El Paso, TX

US Army Electronics Research and Development Command
Atmospheric Sciences Laboratory
White Sands Missile Range, NM 88002

NOTICES

Disclaimers

The findings in this report are not to be construed as an official Department of the Army position, unless so designated by other authorized documents.

The citation of trade names and names of manufacturers in this report is not to be construed as official Government indorsement or approval of commercial products or services referenced herein.

Disposition

Destroy this report when it is no longer needed. Do not return it to the originator.

SECURITY CLASSIFICATION OF THIS PAGE (When Data Entered)

REPORT DOCUMENTATION PAGE	READ INSTRUCTIONS BEFORE COMPLETING FORM
1. REPORT NUMBER: ASL-TR-0110	2. GOVT ACCESSION NO.: AD A116118
3. RECIPIENT'S CATALOG NUMBER	
4. TITLE (and Subtitle): THE MANEUVERABLE ATMOSPHERIC PROBE (MAP), A REMOTELY PILOTED VEHICLE	5. TYPE OF REPORT & PERIOD COVERED: Final Report
	6. PERFORMING ORG. REPORT NUMBER
7. AUTHOR(s): Roberto Rubio, Claude L. Tate, Maynard L. Hill*, Harold N. Ballard, Mike Izquierdo, Carlos McDonald**	8. CONTRACT OR GRANT NUMBER(s)
9. PERFORMING ORGANIZATION NAME AND ADDRESS: US Army Atmospheric Sciences Laboratory, White Sands Missile Range, NM 88002	10. PROGRAM ELEMENT, PROJECT, TASK AREA & WORK UNIT NUMBERS: DA Task No. 1L162111AH71
11. CONTROLLING OFFICE NAME AND ADDRESS: US Army Electronics Research and Development Command, Adelphi, MD 20783	12. REPORT DATE: May 1982
	13. NUMBER OF PAGES: 54
14. MONITORING AGENCY NAME & ADDRESS(if different from Controlling Office)	15. SECURITY CLASS. (of this report): UNCLASSIFIED
	15a. DECLASSIFICATION/DOWNGRADING SCHEDULE

16. DISTRIBUTION STATEMENT (of this Report)

Approved for public release; distribution unlimited.

17. DISTRIBUTION STATEMENT (of the abstract entered in Block 20, if different from Report)

18. SUPPLEMENTARY NOTES

*Applied Physics Laboratory, Johns Hopkins University, Baltimore, MD

**Electrical Engineering Department, The University of Texas at El Paso, El Paso, TX

19. KEY WORDS (Continue on reverse side if necessary and identify by block number)

Remotely piloted vehicle	Electric field
Meteorological sensors	Optical turbulence
Aerosols	Stabilizers

20. ABSTRACT (Continue on reverse side if necessary and identify by block number)

A remotely piloted vehicle (RPV) named the Maneuverable Atmospheric Probe (MAP) has been instrumented with meteorological and aerodynamic sensors to collect aerosol samples and to determine air temperature and pressure (density derived); relative humidity (RH); temperature turbulence structure constants; atmospheric electric field intensity; and aircraft airspeed, angle of attack, altitude, and heading. The aircraft, with a fuselage length of 2.4 m, was designed and constructed for the development of RPV meteorological sensor

DD FORM 1 JAN 73 1473 EDITION OF 1 NOV 65 IS OBSOLETE

SECURITY CLASSIFICATION OF THIS PAGE (When Data Entered)

20. ABSTRACT (cont)

technology that supports US Army research programs related to atmospheric absorption of electromagnetic energy (laser beams). This report documents, in considerable detail, the physical and aerodynamic characteristics of the 10-hp, 36.5-kg, radio-controlled MAP aircraft, as well as the novel fluidic and electrostatic vertical stabilizer systems assisting in aircraft control. The atmospheric and aerodynamic sensor configurations, including the sensor data telemetry system, are described.

Three distinct flight experiments were conducted with the instrumented MAP vehicle. During the first experiment, dust particulate samples, ranging in size from 0.2μm to 400μm, were obtained by flying the RPV-mounted samplers through low altitude dust clouds generated by ground-based 105-mm artillery shell explosions. Data from this experiment are presented. The second experiment involved characterizing typical atmospheric conditions along a laser propagation range (path). Graphs of atmospheric temperature, pressure, RH, and derived air density, all as functions of RPV altitude, present data that are representative of those obtained from the second experiment. Measurement accuracies for temperature, pressure, and RH are respectively shown to be ±1°C, ±2% of the total pressure and ±4% of actual RH. The third experiment was conducted with the instrumented RPV being flown near a mountain peak whose altitude is 2440 m relative to mean sea level (msl). Atmospheric electric field intensity and turbulence structure measurements as functions of RPV position relative to the mountain peak make up the third set of data presented in this report.

CONTENTS

LIST OF TABLES

LIST OF FIGURES

INTRODUCTION

The US Army's Atmospheric Sciences Laboratory (ASL) and the Army Research Office-Durham have jointly sponsored the development of a remotely piloted vehicle (RPV) instrumented with meteorological sensors. The principal objectives of this development were to provide a means of supporting research programs requiring atmospheric data in areas difficult to reach with conventional instrumentation and to concurrently develop a suitable RPV meteorological sensor technology.

Typical ASL research programs that require a meteorological RPV are investigations of the effect of battlefield obscurants on electro-optical (EO) ranging, target detection and surveillance systems, and the characterization of the atmosphere along high energy laser paths. Battlefield studies require in situ multiple sampling of dust and smoke clouds generated by artillery-delivered munitions. Laser weapon programs require meteorological mapping of the atmosphere along specific horizontal and slant paths, including those in close proximity to a mountain cliff. The RPV, instrumented with atmospheric sensors, aerosol samplers, and aerodynamic sensors, was thus configured to serve as a sensor platform capable of satisfying the requirements listed above. It was given the name, the Maneuverable Atmospheric Probe (MAP).

The MAP is radio-controlled. It has a weight of 25.2 kg with a motor that will develop a maximum power of 10 hp and is capable of transporting approximately 11 kg of instrumentation to an altitude of 7.5 km. It is presently instrumented to measure the aerodynamic parameters of airspeed, angle of attack, heading, gust intensity, altitude, and engine revolution rate. Experimental electrostatic and fluidic aircraft stabilizers, along with radio control receiver and sensor signal conditioning electronics, constitute the remainder of the aerodynamic monitoring and stabilization ensemble.

This research project was initiated in October 1978, and preliminary airframe test flights began at the contractor site in April 1979. Fully instrumented test flights were conducted in June 1979 at White Sands Missile Range (WSMR), New Mexico. MAP support of research projects began in July 1979.

The purpose of this report is to describe the entire MAP system in considerable detail, to provide specific examples of MAP research-support flights, and to present corresponding data acquired during these flights. Therefore, the report presents the aircraft configuration, its flight characteristics, and modes of control, as well as a description of the aerodynamic and meteorological sensors, aerosol samplers, and electric field intensity meters that serve as the MAP payload. Signal conditioning, telemetry electronics, and radio transmission systems are briefly described. In addition, atmospheric data-gathering flights are discussed, and samples of the resultant data, with corresponding measurement accuracies, are presented.

MAP CONFIGURATION AND PERFORMANCE

The resultant configuration of the MAP was dictated by two basic requirements: (1) it must have a rigid, air-worthy sensor platform, and (2) this platform must be easily modifiable, to accommodate the various combinations of sensor and electronic packages that would be fabricated to satisfy each particular flight objective.

Accordingly, the MAP aircraft pictured in figure 1a was designed and constructed by the Applied Physics Laboratory (APL) of Johns Hopkins University. This aircraft can be easily disassembled into three major components: the wing, the fuselage, and the horizontal stabilizer-vertical fin assembly. In addition, the landing gear is readily removable. The disassembled vehicle is small enough to fit in a conventional station wagon. The dimensions of the principal components are listed in table 1. Its aerodynamic surfaces are made of polystyrene foam cores with laminated skins of 0.4-mm thick plywood, with fiberglass cloth, in turn, bonded to the plywood. The fuselage is a molded fiberglass-epoxy shell.

TABLE 1. PHYSICAL CHARACTERISTICS OF THE MAP VEHICLE

Wing span	3.05 m
Wing area	1.36 m^2
Fuselage length	2.4 m
Fuselage diameter	22.8 cm
Pod length	70.0 cm
Pod diameter	15.2 cm
Engine weight	5.5 kg
Airframe weight	11.0 kg
Control equipment	3.2 kg
Payload weight	11.0 kg
Fuel weight	5.5 kg
Gross launch weight	36.2 kg

A schematic diagram showing the location of key components is included in the three-dimensional drawing of figure 1b. The fuselage contains a Herbrandson-Dyad 160, 10-hp, 2-cycle gasoline engine, which drives a 36-cm diameter, 56-cm pitch propeller. An APL-developed muffler and exhaust system are attached to the engine's bottom-rear section, to dampen acoustical reverberations that are detrimental to turbulence sensor measurements and to divert engine effluents from the atmospheric sensor area. Behind the firewall is the electronics power supply, which is a 28-V, 5-A battery. Immediately behind and above the power supply is a radar transponder. Directly beneath the transponder is a three-axis fluidic gyroscope. The 5.7-l fuel tank front wall, which is located on the aircraft center of gravity, closes the transponder-gyroscope compartment. Behind the rear wall of the gas tank are the electronics packages for the atmospheric sensors, telemetry, autopilot, and aerodynamic sensors. Further to the rear is a two-axis magnetometer for deriving heading information. A hollow dorsal fin contains the control receiver of the aircraft.

The wing structure supports the majority of the sensors aboard the aircraft. Extending 10 cm forward of the leading edge of the wing are two pairs of turbulence sensors, a Pitot tube, two air temperature sensors, and a yaw gust probe. Located at each wing tip are sensors that contain encapsulated Polonium 210 beads, which ionize the surrounding air, to generate sufficient

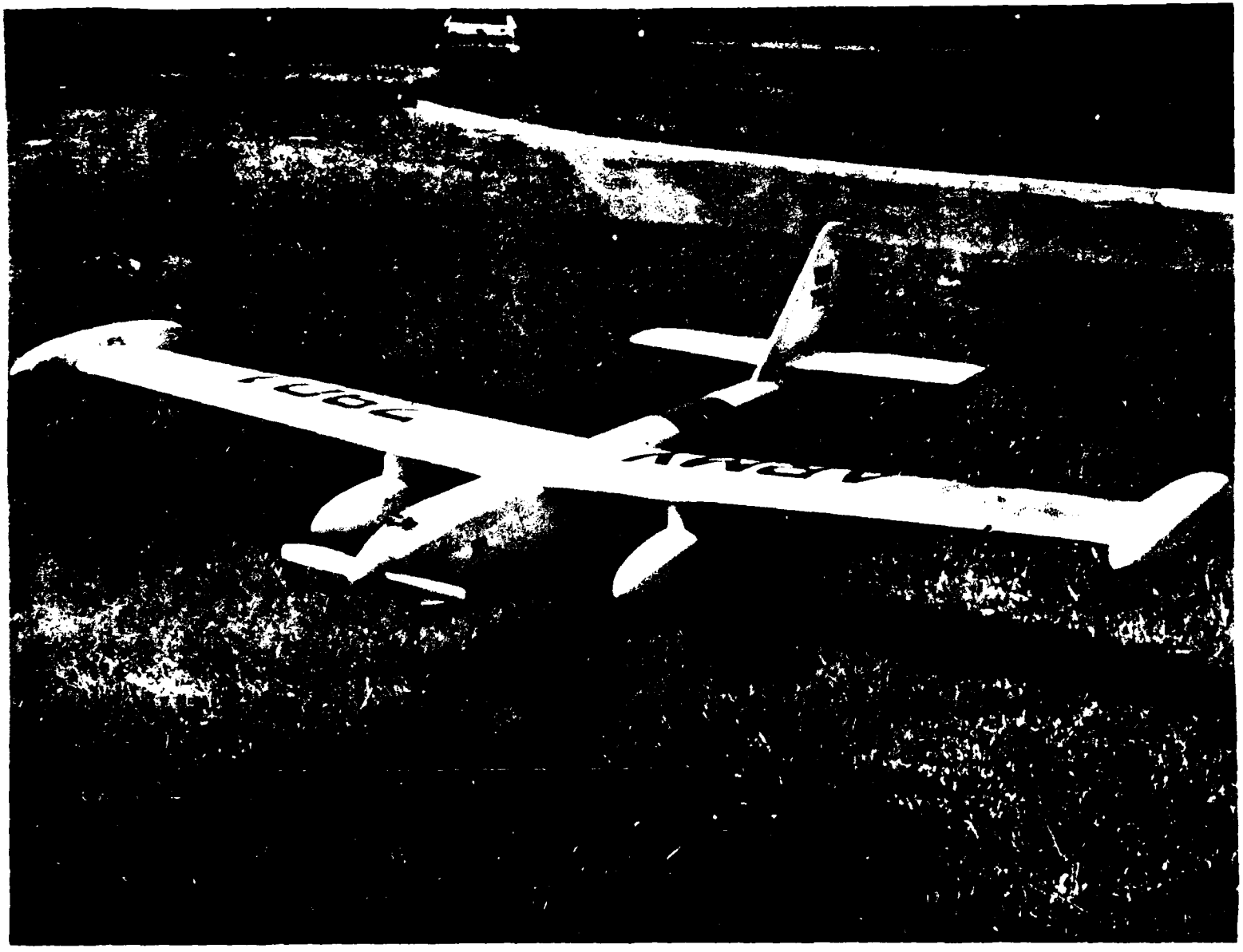

Figure 1a. Remotely piloted MAP vehicle.

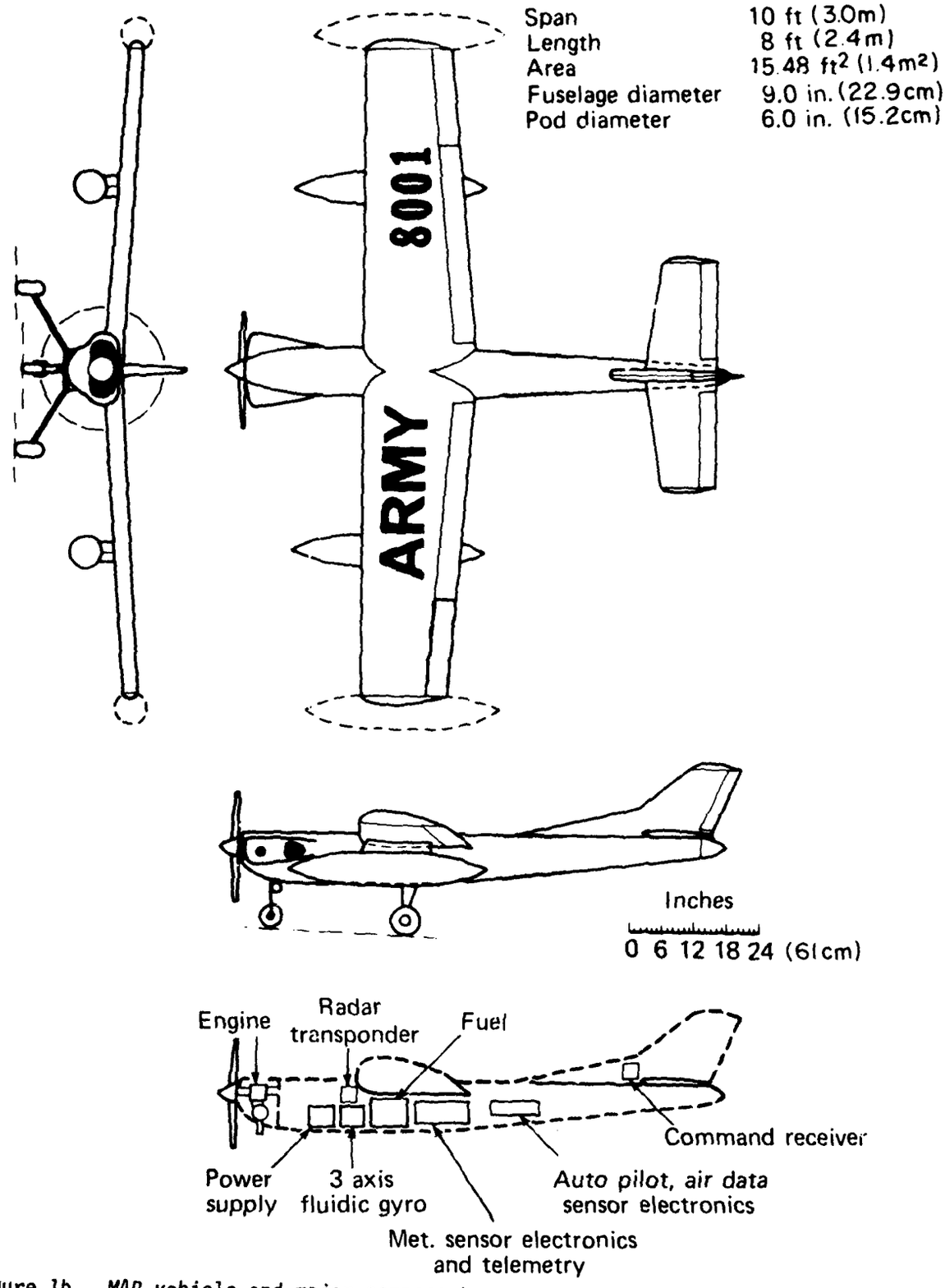

Figure 1b. MAP vehicle and major components.

electric charge for the electric field measurements and to make possible roll electrostatic stabilization relative to the electric field of the earth. Inside the wing, in square and tubular cavities, are the aileron and trim flap control servos, respectively, and all of the electrical wiring that connects the servos and sensors to the various electronic packages.

Suspended beneath each wing, 76 cm from the fuselage axis, is an ellipsoidal pod. Each pod houses an aerosol sampler. Openings in the front and rear sections of each pod permit free air flow through the pod interior.

The empennage unit is made up of a vertical fin and rudder 30 cm in height and a horizontal stabilizer that has an overall length of 1.1 m and contains the servo mechanism for elevator control. The vertical fin contains the rudder control servo.

One Polonium 210 electrostatic ionizer device is mounted on the tip of the vertical fin, while a second one is mounted below it on the side of the fin. These two ionizers, in conjunctions with another mounted on the underside of the fuselage at its aft end, serve to measure the vertical component of the electric field intensity of the earth. The ionizer on the tip of the fin, in association with the ionizer on the side of the fin, also provides electrostatic field pitch stabilization for the aircraft.

A U-shaped aluminum structure 60 cm in length, located beneath the fuselage, supports two air-inflated tires that are 12.7 cm in diameter. This structure is just aft of the aircraft center of gravity, and in association with a spring-cushioned 10.2 cm diameter tire mounted under the engine, constitutes the MAP landing gear. When supported by the landing gear, the underside of the aircraft fuselage is 23 cm above a plane level surface.

Table 2 lists the theoretically predicted aerodynamic performance of the MAP, based upon the aforementioned engine power, aircraft physical characteristics, and payload weight. The test and research flights described in this report have not required that the MAP perform at all the theoretical maximum levels listed in table 2; however, a number of nonrequired test flights that were conducted infer that the theoretical limits are valid.

With a payload weight of 11.3 kg, climb rates of 425 m/min were observed at an altitude of 1770 m above mean sea level (msl). At an altitude of 3660 m msl and with the same payload weight of 11.3 kg, only one-half of the available power was needed to maintain level flight at a speed of 160 km/h for a flight time of approximately 1 h. All of the above data were obtained while flying at WSMR, New Mexico.

Presently, the principal method employed to launch, guide, and recover the MAP relies on visual observation and radio control. Once the aircraft is airborne, electrostatic or fluidic stabilization may be engaged as a control aid.

Aircraft control is effected with a seven-channel Kraft Series KP7-CS/FM, 49.93 MHz transmitter. The transmitter, equipped with a vertical whip antenna, emits an approximate average power of 0.25 W. The signal is pulse-width modulated. The transmitter weighs 0.5 kg and is carried by the pilot while he moves about the flight area to maintain the aircraft within visual

range. The seven channels of the transmitter independently control the (1) power (throttle), (2) internal stabilization (electrostatic, fluidic, or radio control only), (3) pitch (elevators), (4) yaw (rudder), (5) roll (ailerons), (6) lift augmentation (flaps), and (7) engine shutdown (relay release).

Nominal command of the aircraft is via a repetitive 16-ms FM pulse train consisting of eight pulses: one pulse per channel of control information, plus a wide synchronization pulse that separates the seven control pulses.

TABLE 2. PREDICTED AERODYNAMIC PERFORMANCE OF THE MAP AIRCRAFT

Gross weight	36.2 kg
Installed power	7.46 kW
Stall speed at 3.35 km (11,000 ft msl)	65 km/h (flaps)
Stall speed at sea level	58 km/h (flaps)
Minimum power speed at 3.35 km msl	82 km/h
Minimum power speed at sea level	88 km/h
Maximum speed at 3.35 km msl	169 km/h
Rate of climb at 3.35 km msl	244 m/min
Rate of climb at sea level	396 m/min
Practical ceiling	7.6 km msl
Unpowered sink speed at 3.35 km msl	140 m/min
Unpowered sink speed at sea level	122 m/min
Flight duration at 3.35 km msl	1.8 h
Flight duration at sea level	1.4 h
Maximum range at 3.35 km msl	500 km
Maximum range at sea level	418 km

The pulse train is fed to a decoder for routing of the individual commands to the appropriate control servo mechanism. Individual pulses are varied in width to generate proportional commands.

To prevent the MAP from becoming a safety hazard, a fail-safe circuit is also included in the electronics package. The circuit causes the vehicle, while in flight, to automatically enter a controlled failure mode either if the command and control signal is lost or if the on-board receiver power malfunctions. When loss of control signal occurs, the safety circuit commands the engine to throttle to its minimum power setting and then causes the aircraft to enter into a gentle turn of approximately 30-m radius. These actions occur when only two frames of control pulses are continuously lost. If signal reception returns to normal within 15 s, full aircraft power is restored; otherwise, the engine is turned off and the aircraft descends in a tight spiral.

AERODYNAMIC SENSORS

The MAP aircraft contains a variety of sensors that monitor its aerodynamic performance and stabilize its flight. Aerodynamic instrumentation consists of airspeed indicator, tachometer, altimeter, heading magnetometers, and yaw and pitch gust indicators, from which aircraft angle of attack is derived. The remaining aerodynamic instruments are the fluidic gyroscope wing leveler and the electrostatic stabilizer.

Radar tracking of the MAP provides aircraft position as a function of time. A radar transponder aboard the MAP insures a solid radar track when the aircraft is flying close to the ground or in the vicinity of mountainous terrain.

Aircraft airspeed is determined by an Endevco 8503-02 pressure transducer connected to a Pitot tube. The ram pressure intake of the Pitot tube protrudes 15 cm beyond the front edge of the wing, as shown in figure 2. The static intake is integral to the Pitot tube. Both pressures are transferred via plastic tubing to the Endevco gauge inside the fuselage. The gauge is laboratory-calibrated to yield voltage as a function of airspeed.

Engine revolution rates are monitored by an Electro Corporation DI-MAG 58403 magnetic detector. A thin ferrous strip embedded in the engine magneto induces one magnetic pulse per revolution on the DI-MAG detector. Appropriate electronic circuitry is used to count the pulses and to convert the pulse rates to voltage levels proportional to engine revolution rate.

Two DeVelco 9100A magnetometers are used to determine aircraft heading when the wings are level. These devices are mounted at the aft end of the fuselage to isolate them from stray magnetic fields of the engine and electronic circuitry. The magnetometer axes are parallel to the plane's longitudinal (X) and lateral (Y) axes. The DeVelco sensor output voltage is proportional to the angle between the sensor axis and the direction of the horizontal component of the earth's magnetic field. Since the direction of the horizontal component of the earth's magnetic field is a known quantity, and since its magnitude remains relatively constant over the MAP flight altitudes, recordings of the sensor's output voltages yield the aspect angles required to determine aircraft headings.

A simple, but effective, APL-developed gust probe mounted on the top edge of the vertical fin, as shown in figure 3, measures angle of attack and pitch gusts. This probe consists of a low inertia flag whose stem pivots about a potentiometer that is contained in a paraboloid-shaped flag mount. The flag surface is horizontally oriented so that it weatherwaves about an axis perpendicular to the direction of flow. Flag angular deviations with respect to the fuselage (reference) axis, sensed by the potentiometer while in flight, provide a measure of angle of attack. Since the flag swivels freely in response to transient gust impulses, which barely affect the more massive aircraft, the probe also provides pitch gust infomation. The transient signals are interpreted as gust data, while the steady angular deviations yield the angle of attack measurements. An identical probe, as shown in figure 4, is mounted on the front wing with the flag vertically oriented to obtain yaw gust information.

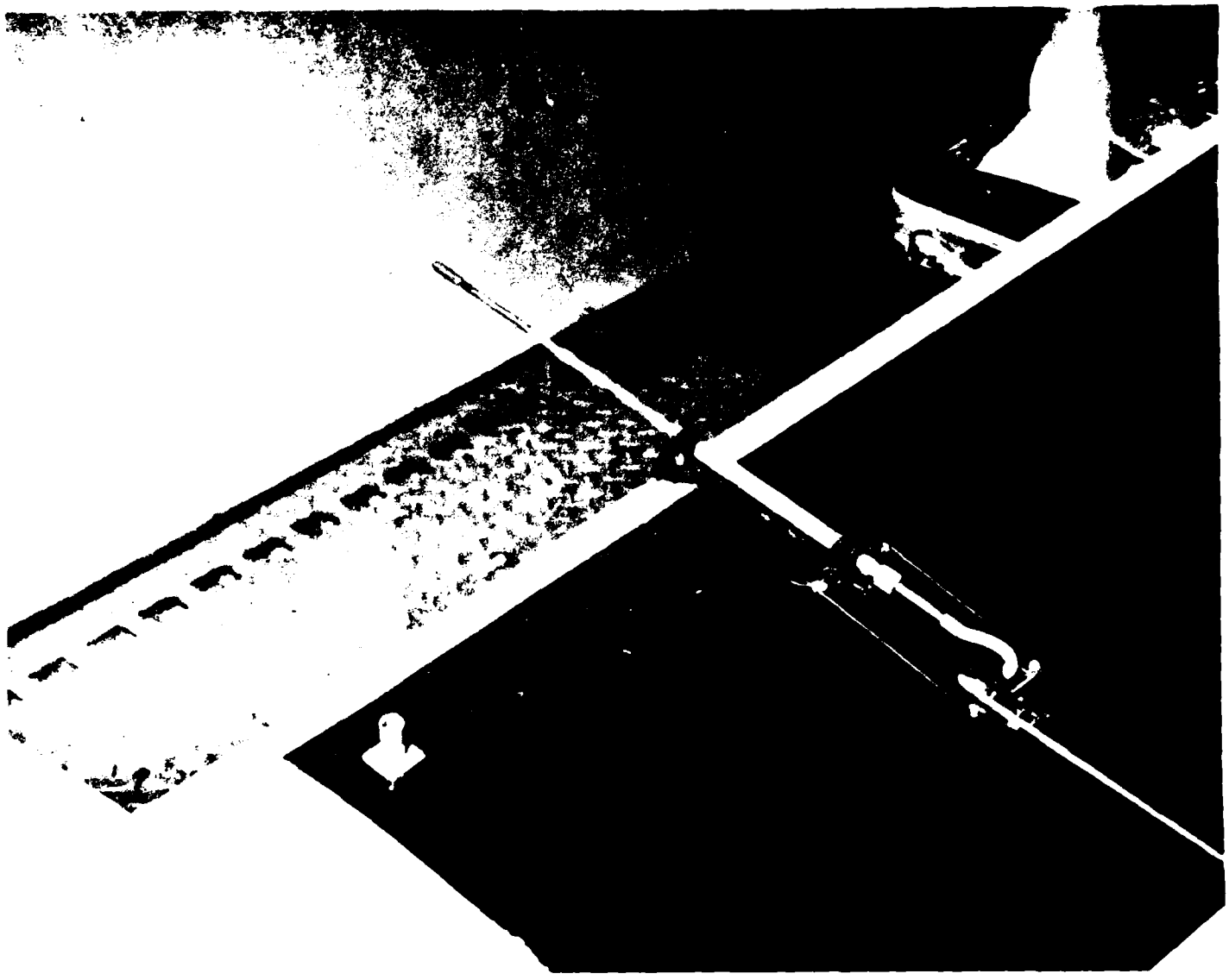

Figure 2. Endevco Pitot tube airspeed indicator mounted below front wing.

Figure 3. Pitch gust probe protruding from top leading edge of vertical fin and Polonium 210 air ionizer on fin tip.

Figure 4. Gulton bead thermistor used to determine air temperature (left) and yaw gust probe (right).

To determine aircraft altitudes independent of a radar track, a National Semiconductor LX1702A atmospheric pressure transducer is included inside the fuselage to serve as an altimeter. The combination of pressure vs altitude and pressure vs voltage calibrations provide a basic response curve of voltage as a function of altitude. Preflight recordings of surface atmospheric pressure, the corresponding transducer output voltage, and the known airstrip altitude supply the information necessary to convert the response curve into a voltage vs altitude calibration.

Exact MAP locations, required to map RPV-measured atmospheric parameters as a function of position, are usually obtained by radar tracking. A WSMR AN/FPS-16 range radar provided component (x,y,z) MAP positions, velocities, and accelerations relative to the launch point. Radar-acquired MAP digital position data is tabulated as a function of time in table 3.

The coordinate system used was the Selected Stationary System. Values of X(s), Y(s), and Z(s) list the location of the aircraft in terms of the east-west, north-south and vertical components, respectively, of its position vector relative to the MAP airstrip center. Time is expressed in seconds Greenwich mean time (Gmt). The columns headed V(x), V(y), V(z), A(x), A(y), and A(z) list values of the aircraft velocity and acceleration components, relative to the airstrip center, while the columns headed Hgt above Terrain and Height list the aircraft height relative to the terrain immediately below and height above sea level, respectively.

A radar skin track of the MAP is quite satisfactory when the aircraft is above intervening buildings and terrain features. However, because the radar skin track of the MAP at low elevation angles is susceptible to considerable signal clutter, a radar transponder was added to the MAP payload. The transponder used is a VEGA model 366C. It has a weight of 0.73 kg and a volume of 410 cm^3. Miniature cables from the transponder feed two TECOM 106002 circular slot antennas (3.1-cm diameter), which are mounted flush on the underside of the fuselage and on the top surface of the wing. The transponder, coaxial cables, antennas, and necessary mounts weigh 1.0 kg. Radiated power is 40 W. The emitted signal is circularly polarized and lies in the 5.4 to 5.9 GHz frequency range.

AIRCRAFT STABILIZERS

A basic requirement for a relatively inexpensive RPV is a compact, inexpensive all-weather stabilization system. Thus, two novel vertical stabilization systems were incorporated into the MAP. One is based upon the principle of electric field sensing, while the other is based upon the principle of fluidic angular rate sensing. The electric field sensor is referred to as an electrostatic autopilot, even though as presently used this device is not an integral part of the MAP altitude and heading sensing capability. The electrostatic

TABLE 3. SAMPLE OF 10 JULY 1980 RPV TRACK

Time s(Gmt)	X(s) m	Y(s) m	Z(s) m	V(x) m/s	V(y) m/s	V(z) m/s	A(x) m/s/s	A(y) m/s/s	A(z) m/s/s	Hgt above Terrain m	Height m(msl)
60027.0	1015.29	-179.20	648.82	-28.364	0.053	1.261	0.5935	-0.2442	1.9624	453.78	2422.21
60028.0	987.22	-179.27	650.86	-27.753	0.242	2.483	0.5774	-0.3301	0.2986	459.15	2424.24
60029.0	959.79	-279.48	653.21	-27.103	0.036	2.029	0.6549	0.8062	-0.9356	464.76	2426.59
60030.0	932.90	-178.95	654.74	-26.830	0.977	1.067	-0.1263	0.7962	-0.8172	469.49	2428.11
60031.0	905.95	-177.61	655.42	-27.123	1.696	0.321	-0.3658	0.6852	-0.7145	473.39	2428.79

autopilot was invented at APL by M. L. Hill.[1] It has been demonstrated that this device performs extremely well in fair weather and in some forms of adverse weather; however, incorporation of electrostatic autopilots into operational all-weather vehicles requires a more detailed knowledge of the earth's electric field structure and variability in extremely dry air, mountainous surroundings, and inclement weather. The electrostatic autopilot development and its basic measurements of earth's electric field intensity are an integral part of the MAP research program. Because of these uncertainties in the variations of the electric field intensity of the earth, and because a commercially available three-axis fluidic gyroscope meets all-weather criteria and is relatively inexpensive and compact, the fluidic gyroscope was made a part of the MAP payload.

An ubiquitous electric field exists in the fair weather portions of the atmosphere, with its positive polarity at the lower boundary of the ionosphere and its negative polarity at the surface of the earth. The corresponding electric field intensity ranges typically from 10 V/m at an altitude of 6 km to approximately 250 V/m at sea level.

Detection of aircraft roll and pitch angles electrostatically is possible because of this vertical gradient in the electric field, with an electric potential difference ΔV existing between any two points differing in height by ΔZ. The vertical displacement of two aircraft extremities (wing tips or nose and tail) produces a height difference ΔZ and a corresponding potential difference ΔV between the extremities. This potential difference is thus proportional to the aircraft roll or pitch angles, and it, in turn, will produce in a conductor connecting the extremities a current that is also proportional to the instantaneous roll or pitch angles.

Four Polonium 210 (Staticmaster model 2U500) alpha particle emitters, each with a source strength of 500μCi, serve to ionize the air surrounding the Polonium device and thus to enhance the current available for detection of roll and pitch angles. These radioactive sources do not present a physical hazard, since each Polonium grain is encased in a protective glass bead, and the bead is then cemented to a substrate encased in a metallic grid. The metallic grid also serves as the conductor that is connected to the atmosphere.

Figure 3 shows a Polonium source mounted on top of the vertical fin to sense pitch angles. Its corresponding pitch voltage output is referenced to the average potential of two identical devices that are mounted on the wing tips to sense roll angles. Copper wiring connects each pair of Polonium grids to a sensitive voltage differential amplifier. Strips of copper tape positioned near the ionizers serve as shields or guards. These are electrically connected to the airframe ground. Outputs from the electrostatic circuitry are filtered, impedance matched, and applied to the respective control servo mechanisms to complete the pitch and roll angle control loop. The electrostatic circuits are physically located in the aerodynamic sensor electronic

---

[1]Hill, M. L., "Introducing Electrostatic Autopilots," Astronautics and Aeronautics, November 1972.

package inside the fuselage. The entire electrostatic circuit, four Polonium units, and the three associated control servos weigh 0.5 kg.

The other MAP stabilization system uses a KGB Corporation model 7603 three-axis fluidic angular rate sensor. Serving as a gyroscope, it has a volume of 785 cm^3 and weighs 0.4 kg. Its principle of operation is based upon the detection of the magnitude of fluid jet deflection that is induced by Coriolis forces when the aircraft is rolling, pitching, or yawing. Three orthogonal laminar flow air jets, each of which flows in a direction perpendicular to the direction of the rotational motion to be sensed, impinge upon a pair of heated thermistors that are aligned in a direction transverse to the rotational axis and lie within the jet stream. The electronics of the fluidic gyroscope continously monitor the differential temperature of the two thermistors. As the aircraft rotates about one of the three orthogonal axes, the jet transverse to that axis is deflected. Correspondingly, one thermistor of the pair is partially removed from the convective cooling effect of the jet stream. This action creates a measurable temperature difference between the two thermistors. This temperature difference is detected and converted to a voltage that is proportional to the angular rate of rotation about the axis. This output voltage, calibrated as a function of angular rate, is then applied to the appropriate control servo mechanisms for aircraft stabilization.

A basic aerodynamic characteristic of most aircraft is an inherent roll-yaw coupling. This characteristic is used to stabilize the aircraft in a wing-level attitude, through use of the fact that the yaw rate can be made zero only when the aircraft is flying with its wings level along a straight-line path. At any time when the aircraft is in a banked turn, its flight path is curved, which produces yawing about its vertical axis. Thus, sensing the yaw rate and then closing a loop to drive the yaw rate to zero will cause the aircraft to fly with its wings level.

This method of wing leveling is substituted for the conventional inertial rate gyroscopes in some general aviation autopilots. It has been under investigation by the National Aeronautics and Space Administration (NASA) and the US Air Force. Some of the results of these investigations were employed at APL in the design of the fluidic system for the MAP vehicle.

Both rudder and ailerons are employed in the wing leveling portion of the MAP autopilot. The direct current output of the yaw rate gyro provides wing leveling, while an alternating component of both yaw and roll rate is used to produce damping.

Stabilization of the MAP about the pitch axis is accomplished by sensing the angle of attack with the pitch gust probe and closing a loop to the elevator sensor, which commands a fixed angle of attack. The pitch rate gyro is used only for damping in the loop, to prevent the aircraft from entering a wild phugoid-type oscillation about its pitch axis. When the aircraft is locked into this fixed angle of attack mode, an altitude hold capability is made possible by simply selecting a throttle power setting consistent with the desired altitude. The desired speed during an altitude-hold maneuver is obtained by changing the trim setting of the elevator. This altitude-hold capability was not operational during the later MAP flights, but the capability was demonstrated when the pilot used only the aircraft throttle and radar altitude readings to maintain a constant altitude during specific experiments.

ATMOSPHERIC SENSORS

The MAP was instrumented with atmospheric parameter sensors that are relatively simple in design and light in weight. RPV sensor technology was developed to determine atmospheric temperature, pressure, RH, temperature turbulence structure constants, and electric field intensity. From these direct measurements, air density and turbulence refractive index structure constants are derived.

This section describes each sensor in considerable detail and gives the precise location of each sensor on the aircraft. The calibration techniques used and the electronic circuits employed to improve sensor measurement accuracy are described and, when available, the measurement accuracy is stated.

Atmospheric temperature is determined with a Gaulton 1-mm diameter bead thermistor mounted 10 cm forward of the leading edge of the left wing and positioned 0.5 m from the fuselage longitudinal axis. This thermistor is shown in figure 4.

A second temperature sensor is positioned 10 cm forward of the right wing leading edge and 1 m from the fuselage axis. Placement of this sensor at the indicated location insures that the air temperature is sensed outside the airflow boundary layer of the wing and that propeller induced effects on atmospheric temperature are negligible. The thermistor and mount weigh 55 gm.

Electrical wire connecting the bead thermistor to the temperature sensor electronics passes through the wing interior. Temperature values are monitored by recording the frequency of an oscillator controlled by the resistance of the thermistor, which varies with temperature. Calibration of the thermistor resistance vs temperature gives atmospheric temperature as a function of oscillator frequency.

The temperature sensor electronics include a means of monitoring oscillator frequency drift due to temperature effects on circuit components, by periodically and alternately substituting two fixed value resistors for the thermistor in the oscillator circuit. One resistor provides a low reference frequency, while the second yields a high reference frequency. Data frequencies, corresponding to the expected range of temperatures measured, are designed to lie between the low and high reference frequency limits. Each data point frequency is accordingly corrected for circuit drift prior to its conversion to a corresponding atmospheric temperature value.

Frequency drift corrections permit temperature measurements to be made with a theoretical accuracy of $\pm 0.5^{\circ}C$ in the altitude intervals of interest; however, realistic accuracy calculations must consider the effects of thermistor bead solar heating and possible aerodynamic heating. Employing techniques developed by Ballard and Rubio,[2] temperature effects induced by solar and aerodynamic heating of the bead and its thin wire mounts were calculated.

---

[2]Ballard, H. N., and R. Rubio, "Corrections to Observed Rocketsonde and Balloonsonde Temperatures," J Appl Meteorol, 7:5, 1968.

Solar heating of the bead was found to be 0.5°C or less for MAP flight altitudes. Typical aerodynamic heating results were as follows: 0.8°C at 130 km/h and 0.3°C at 95 km/h. MAP airspeeds normally ranged between 80 km/h and 130 km/h during a data collection flight. Thermistor ohmic heating is another source of error. By reducing the sensor current to a bare minimum, ohmic heating was reduced to a negligible amount. Based on the above temperature measurement uncertainties, MAP air temperature data may be measured with an accuracy of ±1.0°C without applying temperature corrections. Response time of the bead was also calculated and found to be 0.5 s or less throughout the altitude interval explored by the MAP.

Atmospheric pressure is monitored with a National Semiconductor LX1702A pressure transducer. This transducer is a piezoresistive strain sensor laid out on a diaphragm. As ambient pressure changes vary the strain on the diaphragm, a corresponding output voltage is developed. This dc voltage in turn varies a frequency output signal. Thus, the basic transducer calibration gives frequency as a function of ambient pressure. As is true of temperature, this circuit also contains a high and low reference frequency calibration to correct for circuit drift. The LX1702A sensor is approximately 23 cm^3 in volume, weighs less than 110 g, and was physically located within the sensor electronics package, with the pressure port protruding outside the electronic case into a small empty space between the case and the fuselage wall. Atmospheric pressure measurement accuracies were determined to be within ±2% of the measured pressure value.

To determine RH, conventional rawinsonde carbon hygristors (ML476) are used on the MAP. This device is a cellulose acetate butyrate (CAB) base with carbon particles uniformly distributed. As RH increases, the CAB expands and causes the carbon particles to move further apart, which in turn increases the resistance of the element. When RH decreases, the opposite effect occurs. These changes in resistance, corresponding to RH changes, are used to alter the frequency output of a voltage-controlled oscillator. Calibrations of RH vs resistance and resistance vs frequency are combined to obtain a final calibration of RH as a function of frequency. Low and high reference resistors are again intermittently introduced into the circuit to correct for electronic temperature drift effects.

The RH sensor (85 g in weight) is positioned 1.3 cm below the leading edge of the wing and 40 cm from the longitudinal axis of the fuselage. Since RH measurements are affected by the humidity element temperature, the sensor was placed in this position below the wing to shield it from the direct solar radiation.[3] A measurement error is introduced when the RH element is at a temperature other than ambient temperature. The amount of this error caused by boundary layer heating of the humidity element was found to be negligible when compared to the solar heating effect.

---

[3]Design Review Agenda for Meteorological Sounding System Radiosonde Design, Space Data Corporation, 10 April 1978.

The accuracy of the RH element vs frequency calibration accuracy was established to be within ±3% RH at a specific calibration temperature. Solar heating due to albedo adds a ±0.5% RH inaccuracy. Another inherent inaccuracy is introduced at temperatures other than the calibration temperature, since the device has a slightly different RH response at each temperature. This last inaccuracy can produce a ±2.5% RH uncertainty in the measured RH values within the altitude interval in which the MAP was flown. Consequently, RH measurements made during the MAP flights may have an inaccuracy of ±4% RH. In spite of the ±4% uncertainty, the carbon resistor is easy to use and calibrate, and it furthermore yields values of RH acceptable to meteorologists who obtain similar data with the same sensors aboard rawinsonde balloon-borne instruments.

Two pairs of differential temperature sensors provide a measure of the temperature turbulence structure constants. The sensors are tungsten filaments having a diameter of 7.5μm and a resistance of 220 Ω. They are all mounted 10 cm forward of the leading edge of the wing. One pair of filaments is separated by a distance of 20 cm, while the second pair is 2.8 m apart. Figure 5 shows three of the four turbulence elements. The outermost filament in figure 5 operates in conjunction with an identical sensor mounted on the opposite wing, while the two innermost filaments form the 20-cm turbulence sensor. All four filaments and their associated sensor mounts weigh approximately 215 g. The turbulence elements were sufficiently removed from the propeller (approximately 1 m from the shaft) to avoid engine and propeller effects on the airflow past the sensors.

When the aircraft is flying in a height regime in which the outer scale of turbulence is less than 2.8 m, only the 20-cm sensor will record meaningful data. Thereafter, as the aircraft ascends, the 20-cm sensor signal level decreases until electronic background noise gradually obliterates the signal; however, by this time the data from the 2.8-m separation sensor is meaningful.

Differential temperature values between each sensor pair are determined by placing each element of the pair of filaments as a leg of a balanced Wheatstone bridge. As a turbulence cell flows past a sensor pair, the difference in temperature between the two points in the cell corresponding to the separation of the sensor pair changes the corresponding resistance of each filament, thus unbalancing the bridge. This resistance difference is converted to a proportional output voltage by a differential amplifier. Root-mean-square (rms) values of output voltage from the differential amplifier over 1-s intervals subsequently vary a voltage-controlled oscillator. As a result, the system produces rms differential temperature values between the two thermistor filaments, as a function of oscillator frequency.

A basic calibration is obtained by introducing successive values of fixed resistance into one leg of the Wheatstone bridge and recording the corresponding frequencies of the voltage-controlled oscillator. To convert the changes in resistance to corresponding changes in temperature of the tungsten filaments, use was made of the equation that relates the resistance of the filament to its temperature, namely

$$R = R_0 + \alpha R_0 T \ , \qquad (1)$$

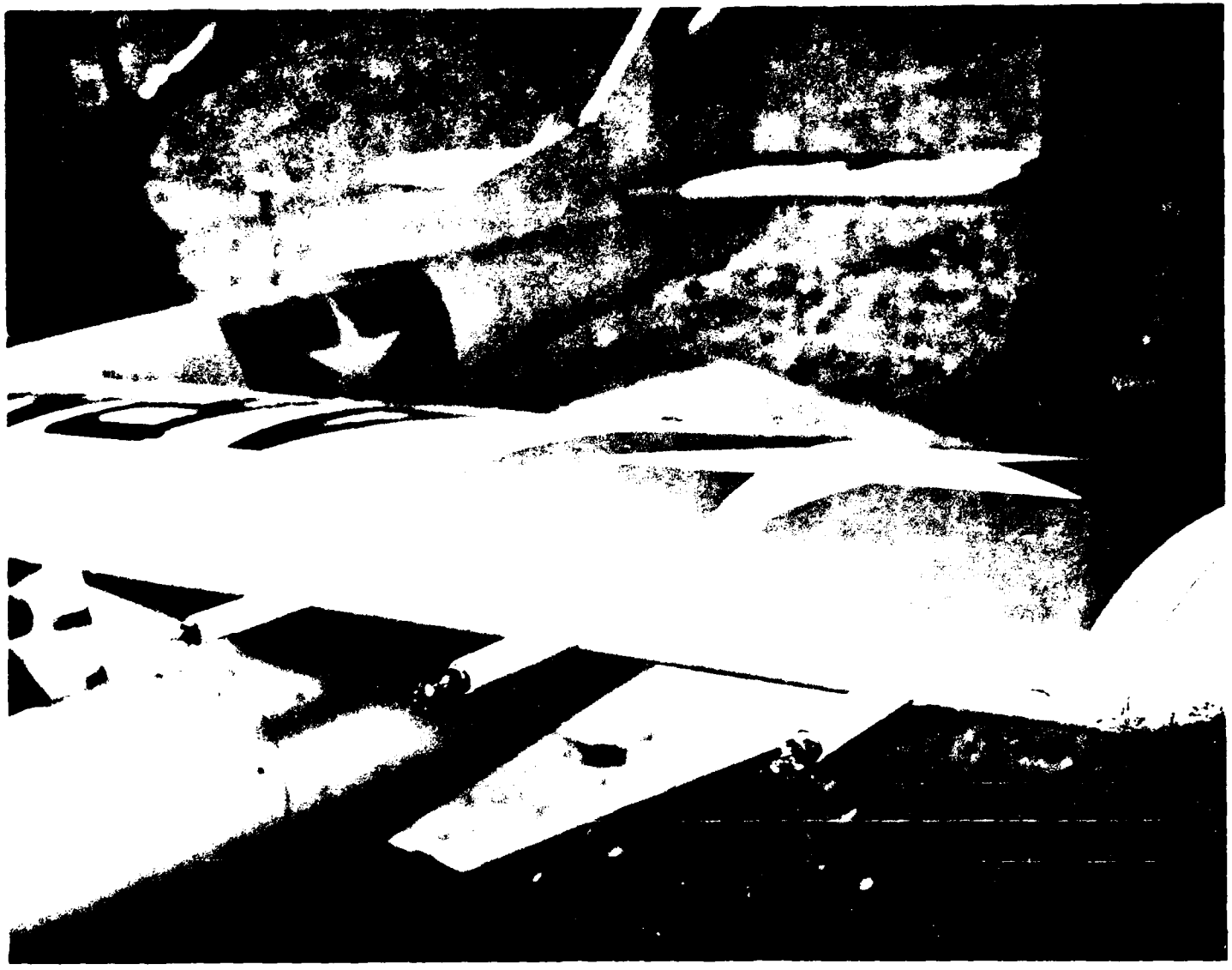

Figure 5. Tungsten filament temperature sensors used to determine 20-cm scale size air turbulence (left and center) and one temperature element of 2-m scale size turbulence sensor (right), all mounted on tip of wing tubular extensions.

which leads to the equation

$$\Delta R = \alpha R_o \Delta T \ , \tag{2}$$

which in turn gives

$$\Delta T = \frac{\Delta R}{\alpha R_o} \ , \tag{3}$$

where ΔT is the change in temperature corresponding to the change in resistance ΔR, R_o is the resistance of the tungsten filament at temperature T_o, and α is the temperature coefficient of resistance for tungsten, equal to $4.5 \times 10^{-3}\ ^\circ C^{-1}$.

Temperature turbulence structure constants, C_T^2, were then calculated from the relationship

$$C_T^2 = \frac{\overline{(\Delta T)^2}}{d^{2/3}} \ , \tag{4}$$

where d is the distance between each element of the temperature sensing pair of tungsten filaments.

The principle of operation of the electrostatic stabilizer on the MAP was discussed under the heading Aircraft Stabilizers. As indicated, the electrostatic stabilizer detects the intensity of the earth's vertical electric field through a determination of the electric field gradient with height, $\Delta V/\Delta Z$. In addition to serving as an aircraft stabilization mechanism, the electric field intensities are independently recorded as potential gradient measurements.

Two Polonium 210 ionization sources, one mounted on the side of the vertical fin and the other below the aft end of the fuselage, are used for vertical electric field measurements. These sensors, in conjunction with the ancillary electronics, provide a measure of the vertical component, E_z, of the electric field intensity of the earth. Similarly, ionization units mounted on the aircraft wing tips generate signals proportional to the horizontal potential gradient in the earth's electric field in a direction perpendicular to the roll axis of the aircraft when the wings of the aircraft lie in a horizontal plane. In addition, signals from the Polonium source on the vertical fin are referenced to the center node of the signals generated by the wing tip ionizers, thus providing a measure of the horizontal component of the earth's electrical field in a direction parallel to the aircraft fuselage axis. Again, these measurements are meaningful only when the aircraft is flying in a straight line at a constant altitude.

The voltage differences measured between pairs of ionization devices, when divided by the measured separation distance between them, provide a measure of

potential gradient in volts/meter. Electric field probe sensitivity is approximately 1 V/m. Vertical electric field intensity values vary markedly with altitude and therefore vertical gradients are easily measured. In fair weather and at aircraft positions distant from buildings and mountains, the horizontal electric field gradients have been found to be minute and are therefore difficult to measure; however, in contrast, in proximity to some types of clouds, in inclement weather, and near mountains or buildings, variations in the horizontal component of the earth's electric field are detectable.

The quantities atmospheric density, ρ, and refractive index structure constant, C_n^2, which are important parameters in the study of atmospheric processes and EO propagation, are not measured directly aboard the MAP, but are easily derived from other parameters measured during the MAP flights. Atmospheric density is obtained through the equation of state for an ideal gas. The atmospheric density, to include the contribution of water vapor to the dry air density, is given by the equation

$$\rho = \frac{PM}{RT} \cdot \frac{(1 + w)}{(1 + w/\epsilon)} , \tag{5}$$

where P is the atmospheric pressure, M is the molecular weight of dry air, R is the universal gas constant, T is the air temperture in degrees Kelvin, w is the mass of water vapor per mass of dry air (mixing ratio) and ϵ is the ratio of the molecular weight of water to the molecular weight of air. Having determined C_T^2 in equation (4) and having measured atmospheric temperature and pressure, C_n^2 is obtained through the equation

$$C_n^2 = \left[\frac{79P}{T^2} \times 10^{-6}\right] C_T^2 . \tag{6}$$

where P is expressed in millibars and T is the Kelvin temperature of the atmosphere.

PARTICULATE SAMPLERS

Timely in situ probing of simulated battlefield obscurants such as smoke, dust, and counter-measure gases, or of natural obscurants such as aerosols, can be effectively conducted with particulate samplers aboard an RPV that can penetrate the obscurant formations. For this purpose, two types of particulate collectors were constructed and fitted inside the MAP wing pods.

The primary sampler used is a multistage impactor designed to collect a fixed amount of sample, wherein the sampling time is dictated by either the length of a laser transmission path or by the spatial dimensions of an obscurant cloud. The other sampler, a Proton Induced X-ray Emission (PIXE) I-1 cascaded impactor, was occasionally flown to acquire general background information regarding the chemical elements that are predominant in atmospheric aerosols

of certain size intervals.[4] Both samplers must be recovered for impactor laboratory aerosol analysis. Photographs and chemical element analysis of the multistage impactors is performed with a scanning electron microscope (SEM). Cascaded impactor samples are analyzed with a PIXE analyzer. The final aerosol data products are particulate shapes and sizes, size distributions, and the elemental composition data.

The multistage sampler contains six elliptical pieces of adhesive cellulose (clear scotch tape) material, each approximately 1.25 cm wide and 2.5 cm long, spaced approximately 1.6 cm apart around the periphery of a teflon cylinder. This cylinder fits inside an outer teflon cylinder with one elliptical window, through which individual collectors are exposed sequentially by rotation of the inner cylinder. A stepping motor and ancillary electronics encased in the bottom half of the inner cylinder rotate each cellulose impactor into the exposed position upon command. The 12 cylinder positions are arranged so that, between exposures, all collectors are covered. The multistage sampler assembly displayed in figure 6 is mounted in a wing pod that has both its front and back conical sections removed to allow free airflow through the pod interior. The sampler axis is oriented perpendicular to the pod axis so that particles can impact directly on the adhesive material as the aircraft flies through the designated air space. Exposure and closure of a collector is controlled from ground level with a second KP7-CS Kraft transmitter operating at a frequency of 49.6 MHz, which is slightly different than the aircraft control frequency. Sampler rotation commands are simple pulses that are acquired by the aircraft control receiver and fed to the stepping motor electronics. The 6.6-cm diameter multistage sampler and enclosed electronics have a volume of 1807 cm^3 and a weight of 0.6 kg. The wing pod and its suspension pylon weigh 0.4 kg.

Aerosol chemical elemental content and surface images are readily obtained by an SEM. Multistage impactor collector strips are analyzed with an International Scientific Instruments Model Super-3A SEM, which is located at the White Sands NASA Johnson Test Facility. In this instrument, an electron gun bombards the particulates and induces secondary electron and X-ray emission. The secondary electron energies are used to form images of aerosol surfaces, which are subsequently photographed for sizing purposes. The X-ray emission spectrum from each particle surface contains wavelengths and wavelength amplitudes characteristic respectively, of the particle's chemical contents and the percentage content of each element. Chemical analysis is performed with an Energy Dispersive X-Ray Analyzer (EDAX).

A photograph and the chemical analysis results of one dust particle are shown in figure 7. This SEM and EDAX system is normally adjusted to provide a spectrum of elements with atomic numbers greater than that of fluorine. Collected aerosols that contain elements with atomic numbers less than 18 may not appear in the aerosol data shown in this report. Particle shapes, sizes, and size distribution in the 0.4μm to 400μm range of particle sizes are obtained from the SEM photographs.

---

[4]Manufacturer's brochure on Cascade Impactors, PIXE International Corporation, P.O. Box 2235, Tallahassee, Florida 32304.

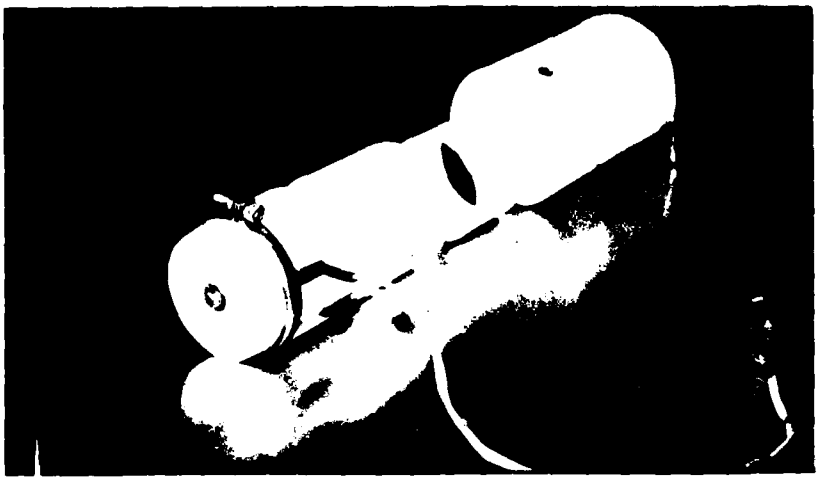

Figure 6. Multistage sequential aerosol collector assembly (inner cylinder) and housing cylinder with collector exposure window.

Element	% Weight
Na	10.4
Mg	7.1
Al	10.1
Si	21.1
S	1.1
Cl	1.4
K	6.4
Ca	33.1
Fe	9.3

Figure 7. Scanning electron microscope image of one dust particle collected with multistage impactor. Particle dimensions are approxiately 12μm wide and 30μm long. Chemical elements, by percent weight, found in this particle are listed.

The PIXE cascaded impactor, model I-1, consists of seven stages of the cylindrical inertial impactor and a final after-filter stage. The PIXE impactor is 7.6 cm in diameter, has a volume of 5080 cm^3 and a weight of 0.7 kg. Figure 8 shows the PIXE sampler, its teflon case, and the frontal cup section of the aircraft pod through which a piece of nylon tubing is fitted to allow air to flow into the sampler. Inside the sampler, at the center of each interior nozzled cylinder, is a thin mylar collector. Annular spacing between the mylar disk and nozzle wall allows air to flow around the collector into the next stage. Operation is based upon the principle that particles of certain masses (sizes) moving at a given speed can change direction and circumvent the centered disk, while larger particles with the same speed but greater mass will impinge on the collector. A vacuum pump attached to the after-filter stage constantly draws air through the seven-stage runcinate tunnel at a rate of 1 m/s. This aerodynamic filtering process results in the first stage collecting particles with sizes of 16μm or greater. Progressively, the following stages filter aerosols with sizes of 8μm, 4μm, 2μm, 1μm, 0.5μm, and 0.25μm. The after filter collects all remaining particles of sizes greater than 0.06μm.

A Brailsford and Company TD-4X2 pump serves as the impactor pump. It is T-shaped, has a volume of 155 cm^3, and adds 0.65 kg to the payload weight. It was also fitted within the wing pod.

PIXE analysis of the aerosols on each mylar disk provides an identification of the elements contained in the aerosol and the total elemental mass for that particular size interval.[5] The X-ray emissions yield a spectrum with peaks located along abscissa channel numbers that correspond to atomic mass number. The amplitudes of each peak, relative to a background level, can be interpreted to determine the element's total mass. Figure 9 shows the spectrum of the aerosols on the first stage disk (sizes > 16μm) that were obtained over desert terrain on the afternoon of 17 August 1979. The smooth downward sloping line in figure 9 is a curve fit to the backgrcund level emissions. For the sample represented by figure 9, the PIXIE analyzer was set to detect elements of atomic number 13 or greater.

SENSOR AND TELEMETRY ELECTRONICS

Atmospheric sensor signal conditioning is performed with circuitry designed and developed by the University of Texas at El Paso's (UTEP) Electrical Engineering Department.[6] APL developed the signal conditioning circuits used with the aerodynamic sensors. All modulation and telemetry electronics were handled by UTEP. Consequently, the atmospheric sensor and telemetry electronics

---

[5]Nelson, J. W., Proton Scattering Analysis for Light Elements in Air Particulate Matter, Report EPA-600/2-78-213, Environment Sciences Research Laboratory, 1978.

[6]Maneuverable Atmospheric Probe/North Oscura Peak Experiment, Schellenger Research Laboratory Report No. FRI-80-UA-89, The University of Texas at El Paso, El Paso, TX, 1980.

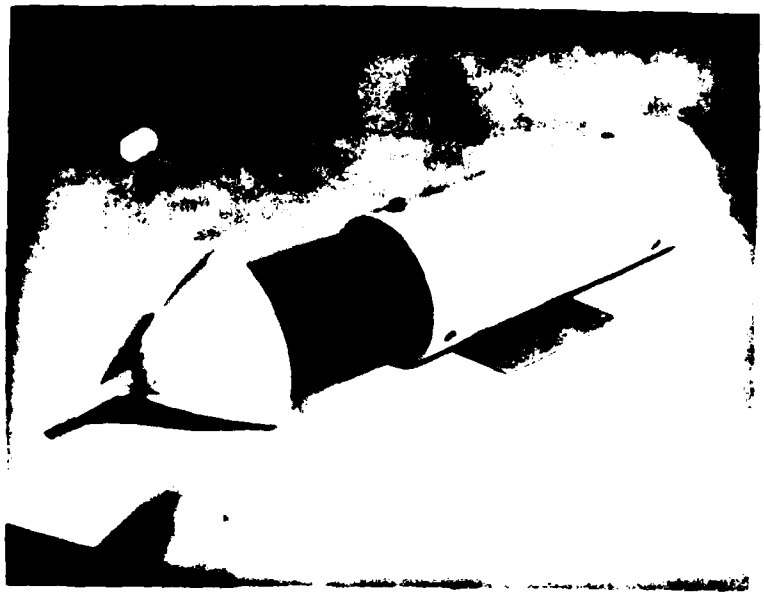

Figure 8. Cascaded PIXE impactors, housing cylinder and wing pod front end cup with aerosol inlet plastic tubing.

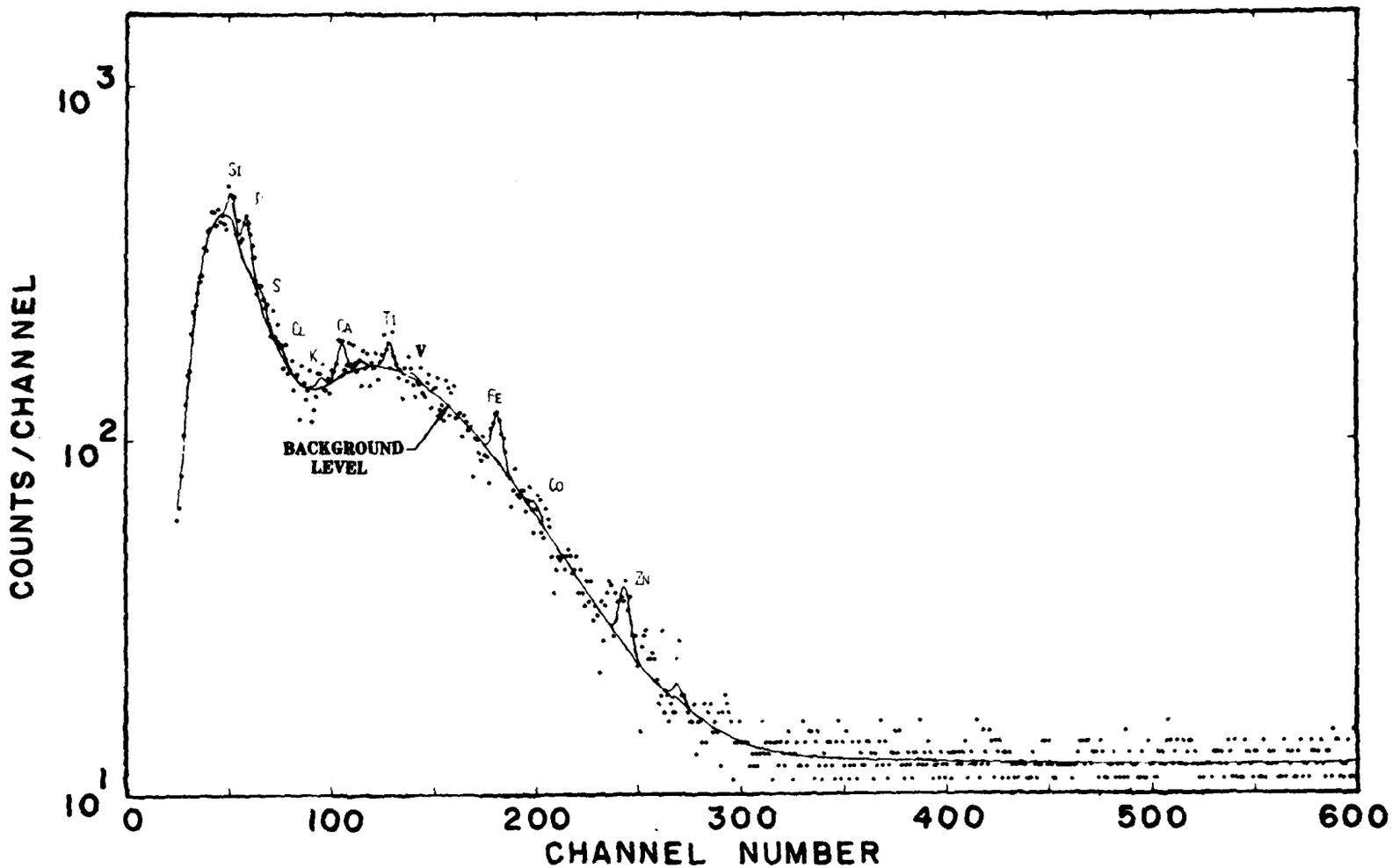

Figure 9. Counts per element spectrum resulting from PIXE analysis of one impactor aerosol sample collected on 17 August 1979 at WSMR, NM. Sample contained aerosols of diameter 16μm or greater.

were contained in one chassis, while the aerodynamic sensor electronics were in a second chassis. These two electronics packages are adjacent to each other within the fuselage. Figure 10, a photograph of the APL electronics, shows an array of six multipin sockets used to interface with the UTEP package, which is comparable in size and weight to the APL package. The APL electronics assembly weighs 1.2 kg and has a volume of 2700 cm^3.

MAP electronic component selection and assembly was made small and light without miniaturization of the circuits. A rationale against miniaturization was adopted because the MAP was to be a research platform; therefore, recurrent changes in sensor requirements, imposed by varying flight objectives, would make it necessary to periodically reset circuit parameters such as sensitivity, amplification, and bandwidths. Without miniaturization, these periodic changes would require only hands-on retuning; with miniaturization, they would require replacement of components. The former approach was chosen. All components were soldered and not socketed, to avoid dislodging of components due to aircraft vibration. Each aluminum chassis was shock-mounted on grommets to minimize vibration-induced electrical noise.

The general flow, modulation, and transmission of sensor signals are illustrated in the block diagram of figure 11. Atmospheric sensor signals are conditioned to output a dc voltage from 0 to 5 V. The dc voltages are fed to IED H-75 voltage-controlled oscillators (VCO), which generate a proportional standard Inter Range Instrumentation Group (IRIG) subcarrier frequency. The conditioned aerodynamic sensor dc voltages are sampled by a 30-bit commutator, which multiplexes the signals before they are applied to one of the IRIG channels. Thus, the aerodynamic sensor subcarrier channel is modulated by discrete pulse amplitudes, rather than continuous dc levels. Thereafter, outputs from all the VCO's, IRIG channels 6 through 19, frequency modulate a 1526.5 MHz transmitter. Three spare channels, 16, 18, and 19, currently exist in the aircraft electronics. Figure 11 shows data on channels 16 and 18 that were used to monitor the instantaneous turbulence signals.

The 1526.5-MHz transmitter is an Aydin Vector T605L, 0.5-W emitter that drives the L band turnstile antenna shown in figure 12. This antenna is normally mounted 3 ft from the aircraft aft end, beneath the fuselage, to avoid airframe obstruction of the radiated signal. In figure 12, the turnstile antenna is above the fuselage. This configuration was chosen for flights during which the ground-based receiver was on a mountain peak above the aircraft.

A 5-Ah power pack composed of Yardley silver-zinc rechargeable batteries supplies a primary voltage of 28 V to the fluidic gyroscope, transmitter, VCO's, PIXE pump, and a dc-to-dc converter. The converter output voltages of $\pm$15 V and +5 V serve to power all other MAP electronic systems and sensors. The receiver and servo mechanisms are powered by a separate 4.8-V NiCad battery. Total system current consumption is 2 A/h, thus permitting a 2.5-h time of operation when all instruments and electronic systems are used. The battery package weighs 3 kg and has a volume of 2050 cm^3.

Ground reception of the telemetered data from the MAP is accomplished by using either the telemetry facilities of WSMR or a van-mounted tracking and recording unit that was developed for off-range flights of the MAP. The Telemetry Acquisition System (TAS) or the Transportable Telemetry Acquisition System

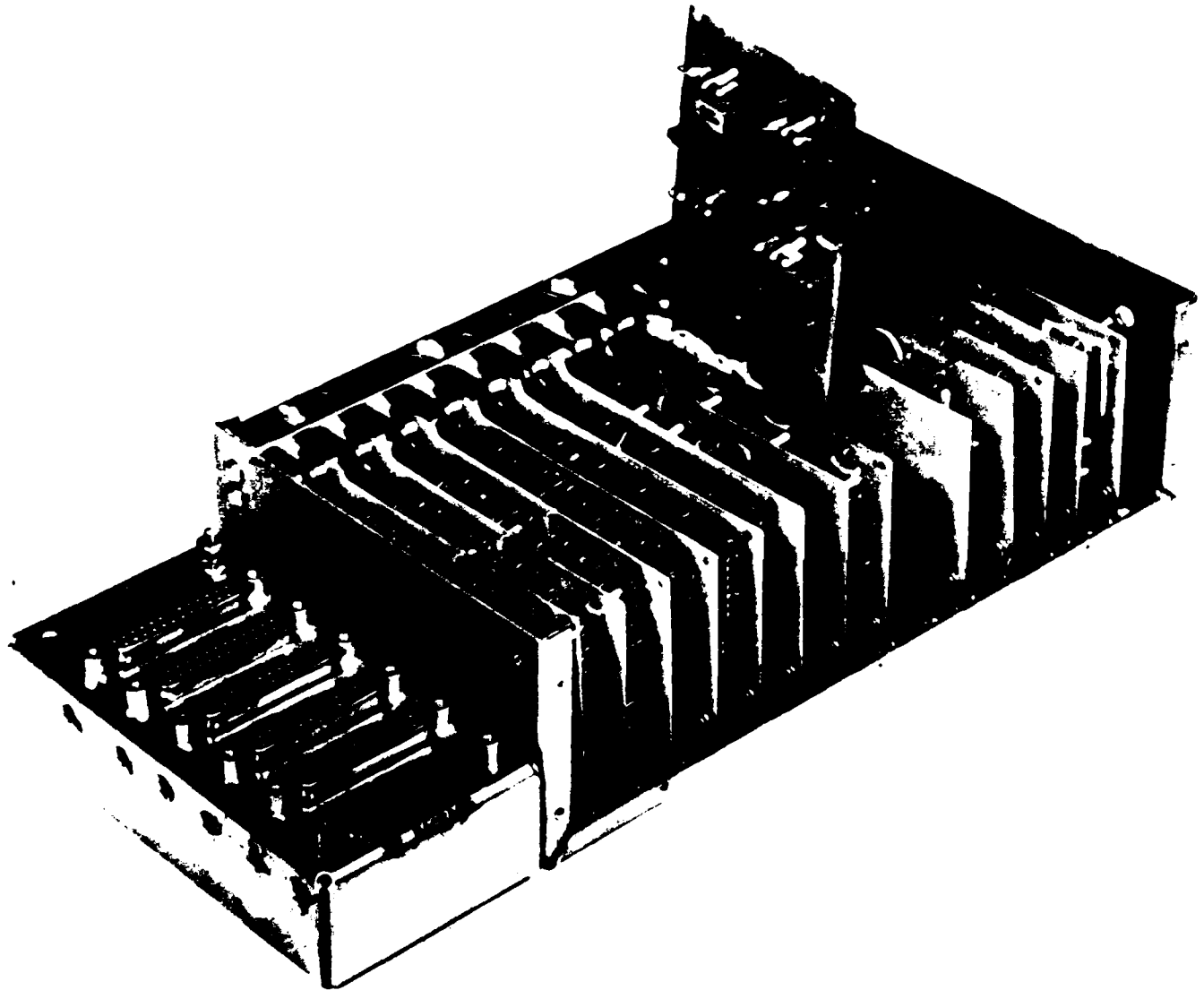

Figure 10. Aerodynamic sensors, electric field intensity, and electrostatic autopilot electronics package.

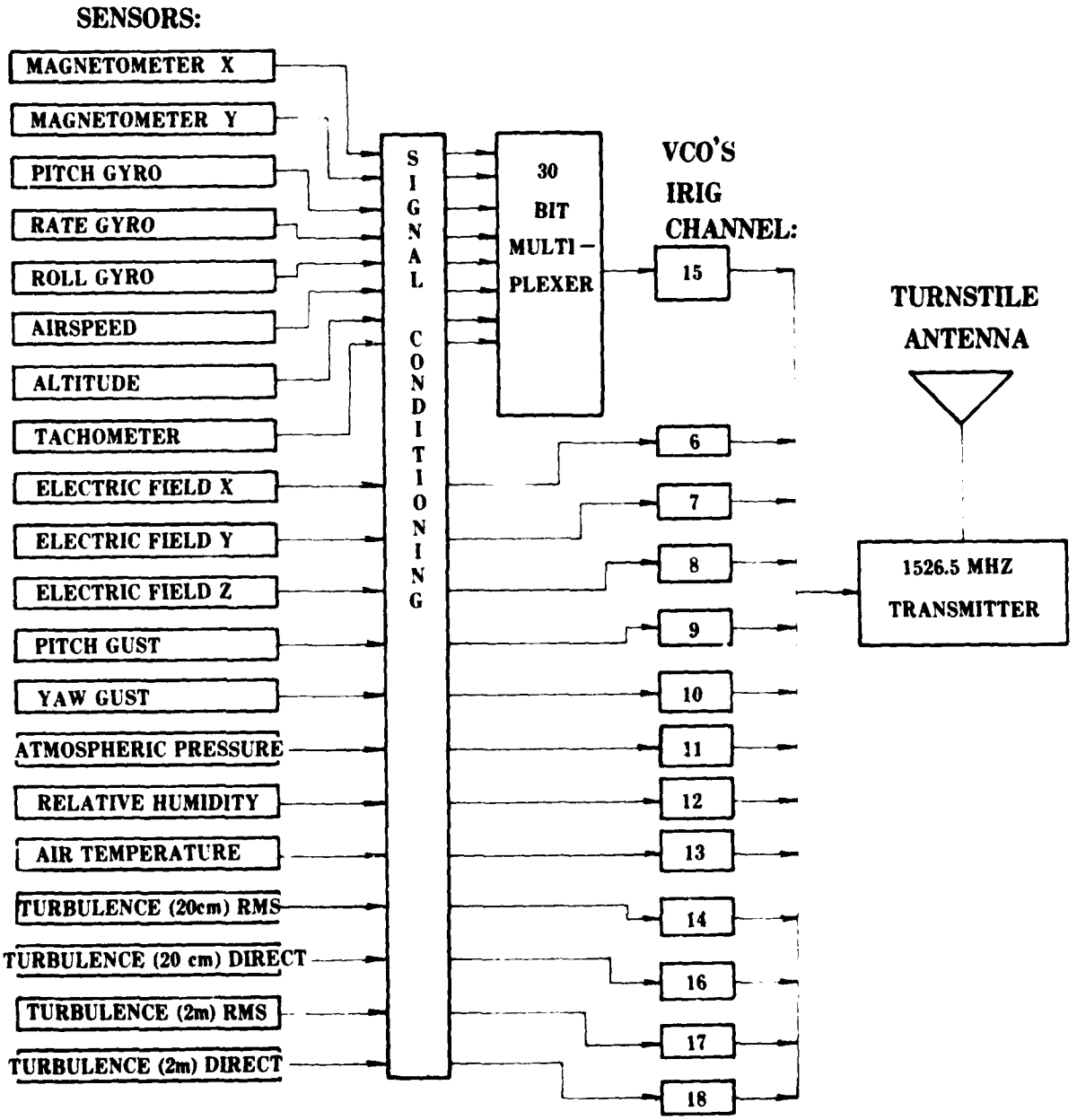

Figure 11. Block diagram depicting sensor signal flow, modulation, and transmission scheme.

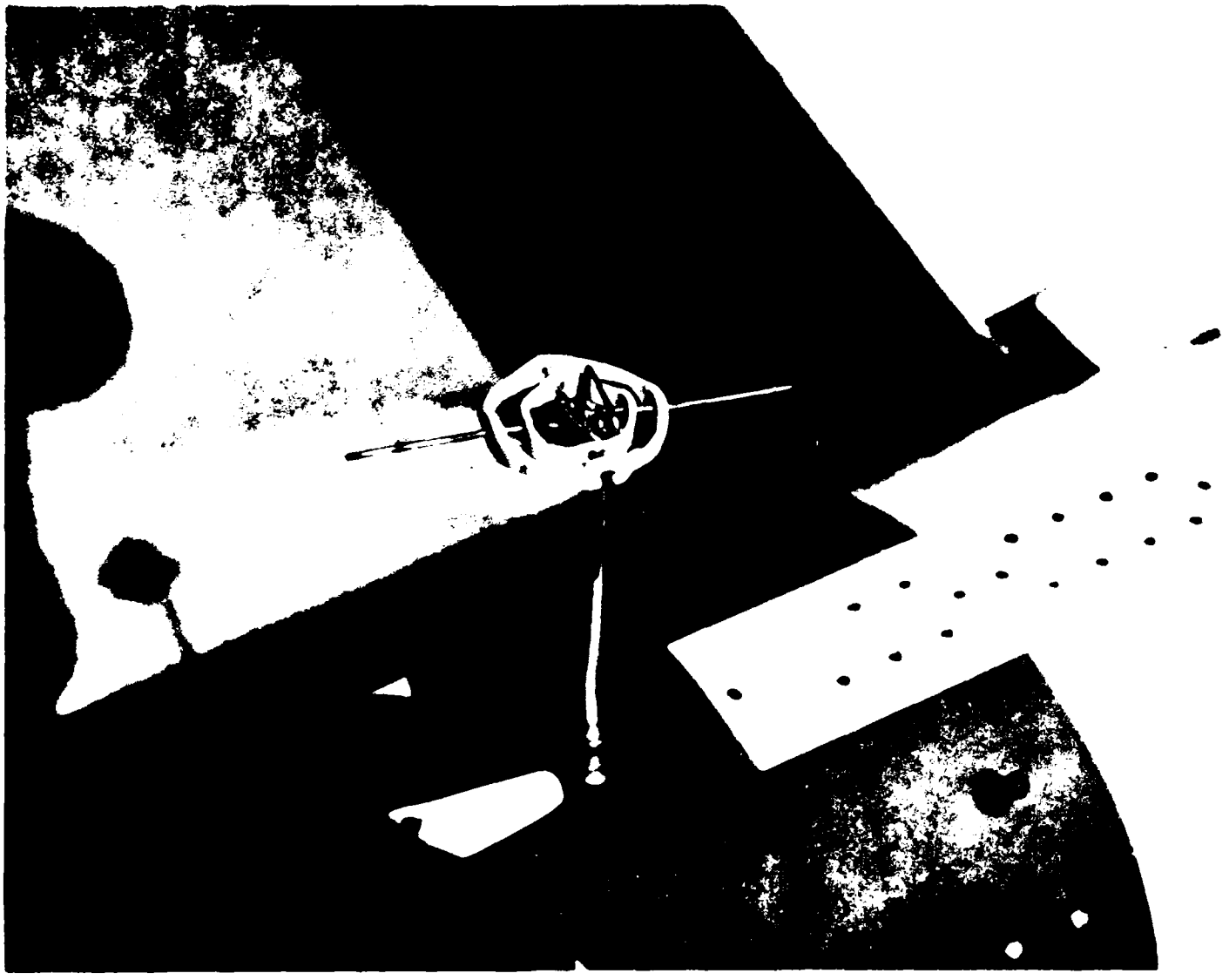

(TTAS) of WSMR offers a variety of modern telemetry support equipment that is described in detail elsewhere.[7]

The off-range data acquisition system developed by UTEP under contract to ASL is, by design, simple and compact. A 1.2-m diameter parabolic reflector antenna is used to track the MAP. The antenna is constructed of aluminum-coated polystyrene, which is light and can be easily steered manually. During MAP missions, the parabolic antenna is mounted on a support frame situated either on the ground or on top of a mobile van that houses the remainder of the ground signal reception equipment. An Astro Communications Lab (ACL) Type SR209 receiver, a bank of Electrical Mechanical Research (EMR) subcarrier discriminators, a selectable four channel voltage display unit, and a Sabre II Sangamo Analog tape recorder make up the remainder of the data-acquisition system. A separate log-periodic antenna and receiver are used to acquire WSMR-transmitted IRIG B timing signals needed to synchronize the telemetry data with the MAP radar position data. For off-range tests time data is internally generated.

SAMPLE FLIGHTS AND ATMOSPHERIC DATA

Three flights that exemplify the versatility of probing the atmosphere with the remotely piloted MAP vehicle are described in this section. Samples of different types of atmospheric data acquired during each of the flights are presented.

A research project entitled "Dusty Infrared Test-II (DIRT-II)" was conducted at WSMR in July 1979.[8] The DIRT-II experiment consisted of a series of artillery shell explosions designed to allow the characterization of dust particulates and formations and to simultaneously measure dust obscuration effects on infrared and near millimeter wave propagation. Sampling of the dust clouds was conducted with the MAP multistage collector. On 25 July 1979, three samples were obtained from a dust cloud produced by a 105-mm shell detonation. The aircraft was launched from a small clearing, and once it was airborne, MAP control personnel took cover behind a bunker until the detonation occurred. After the explosion, control personnel waited momentarily to allow shell shrapnel to clear the test area and then moved from behind the bunker and guided the aircraft through the dust formations.

Figure 13 shows the MAP entering the dust cloud. Just prior to the aircraft's entry into the dust formation, a collector strip was exposed; immediately after the aircraft emerged from the cloud the same strip was rotated into a covered position. An SEM photograph of a small section of the collector strip

---

[7]Telemetry User's Handbook, Department of the Army, White Sands Missile Range, NM, 1 January 1977.

[8]Kennedy, B. W. et al, Dusty Infrared Test-II (DIRT-II) Program, ASL-TR-0058, US Army Atmospheric Sciences Laboratory, White Sands Missile Range, NM, 1980.

Figure 13. MAP aircraft entering dust upheaved by a 155-mm shell explosion for the purpose of collecting dust samples.

used during the first MAP penetration of the cloud is shown in figure 14. This sample was collected 20 s after the detonation, at a height of approximately 25 m. Three particles in figure 14 are labeled, the labels giving the chemical elements found in the particles. Elements other than the oxides were detected by the SEM; the oxides were inferred.

A preliminary particle "diameter" size distribution, deduced from SEM photographs of samples acquired during the third aircraft pass through the same dust explosion, is plotted in figure 15. Particle sizing was done by the Martin technique, whereby the horizontal dimension is measured at the vertical center of each particle. This technique is based on the fact that if the statistical sample (number of particles) is sufficiently large, the random orientation of the particle cross-sectional views yields a meaningful measure of size distribution. Particle size distributions are used to evaluate and improve electromagnetic wave obscuration prediction models.

Another series of MAP flights was conducted in August 1979 for the purpose of mapping atmospheric parameters over a laser beam propagation range. A paved airfield close to the laser range facilitated the launching and recovery of the RPV. Meteorological data was acquired and recorded through use of the ASL transportable ground equipment. Aircraft position data was obtained by an AN/FPS-16 radar skin track of the MAP. The radar transponder had not yet been incorporated into the MAP payload at this stage of its development.

On 17 August 1979, flight patterns were executed to collect data at different altitudes and along slant and horizontal atmospheric paths over the laser range. Atmospheric temperature, pressure, and RH were measured. Air density was derived through the use of equation (5). Graphs of aircraft altitudes and corresponding atmospheric temperature and pressure as functions of time are shown in figure 16. The dots appearing at 1443 and 1445 MST are temperature and pressure values measured by radiosonde sensors when they were at the same altitude as the MAP. Figure 17 is a graphical presentation of the RH measurements obtained aboard the MAP at the same time as the temperature and pressure measurements shown in figure 16. Inspection of both figures shows that temperature, pressure, and RH values measured aboard the MAP were in fair agreement with the limited radiosonde sensor measurements available for comparison.

Note in both figures that at 1435 MDT, on the altitude vs time plots, the radar skin track of MAP was lost as the plane descended to a low altitude. Such losses of RPV position data prompted the incorporation of the radar transponder into the MAP instrumentation system.

A graph of derived air density is shown in figure 18. One plot of figure 18 shows atmospheric density as a function of time as the MAP aircraft first descended slowly at a rate of 30 m/min and then flew at a relatively constant altitude. The other plot shows air density as a function of time as the aircraft ascended at a rate of approximately 17 m/min while traversing a slant path 3 km in length.

During the time that the above temperature, pressure, RH, and density data were obtained, the PIXE Cascade particle impactor was opened for a period of 1 h to collect an integrated sample over the altitude interval extending from the earth's surface to 700 m above it. The temperature was warm, the winds

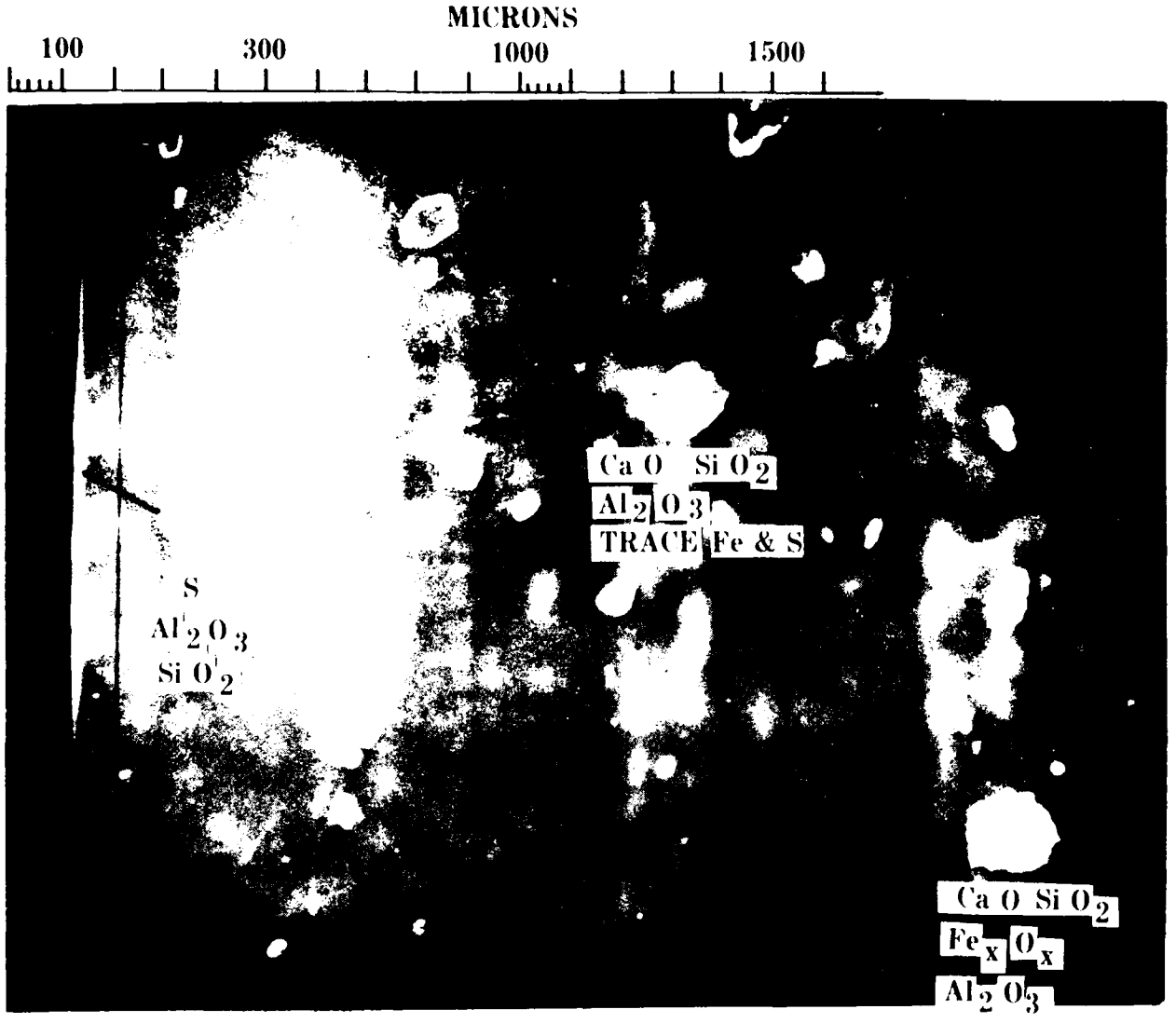

Figure 14. DIRT-II MAP samples from dust clouds.

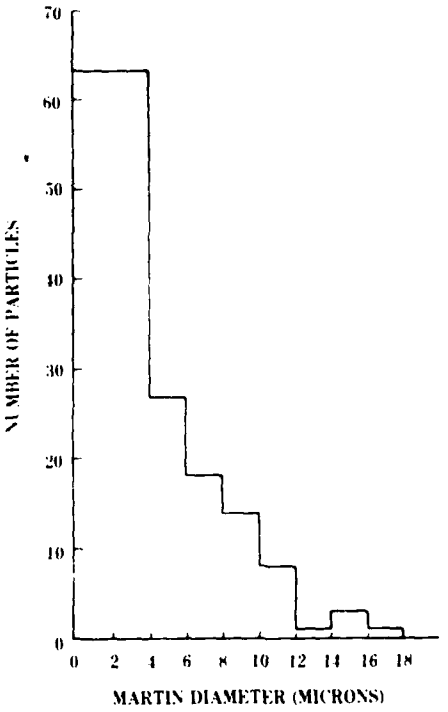

Figure 15. Particle size distribution at 500X magnification from the third impactor pass through the DIRT-II 105-mm explosion.

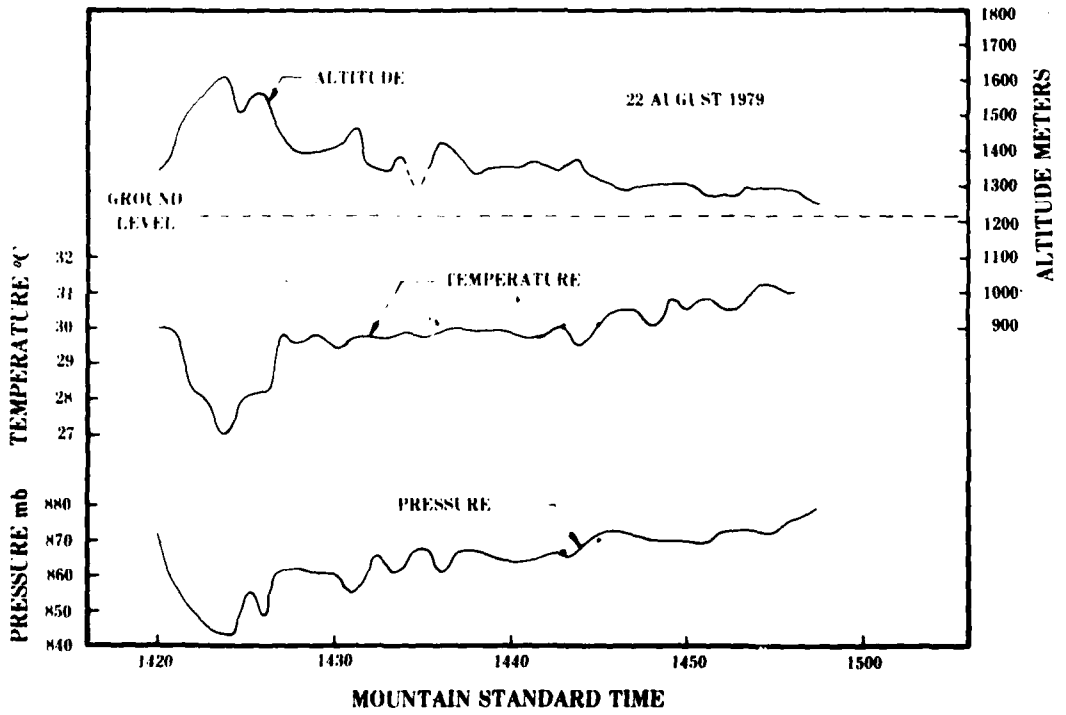

Figure 16. Atmospheric temperature and pressure recorded on board the MAP aircraft and shown as a function of time and aircraft altitude.

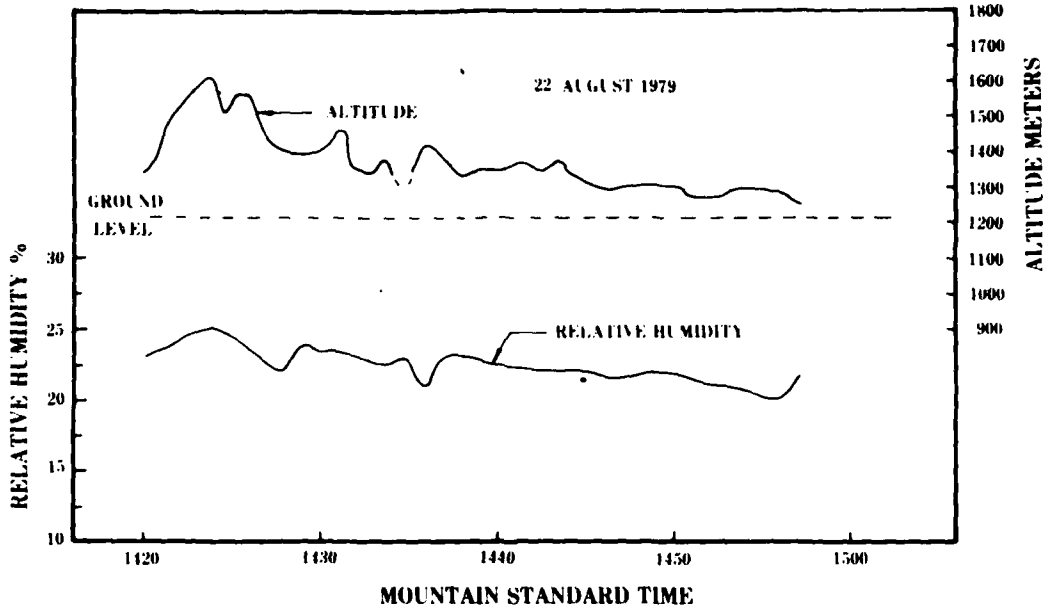

Figure 17. MAP RH measurements as a function of time and aircraft altitude.

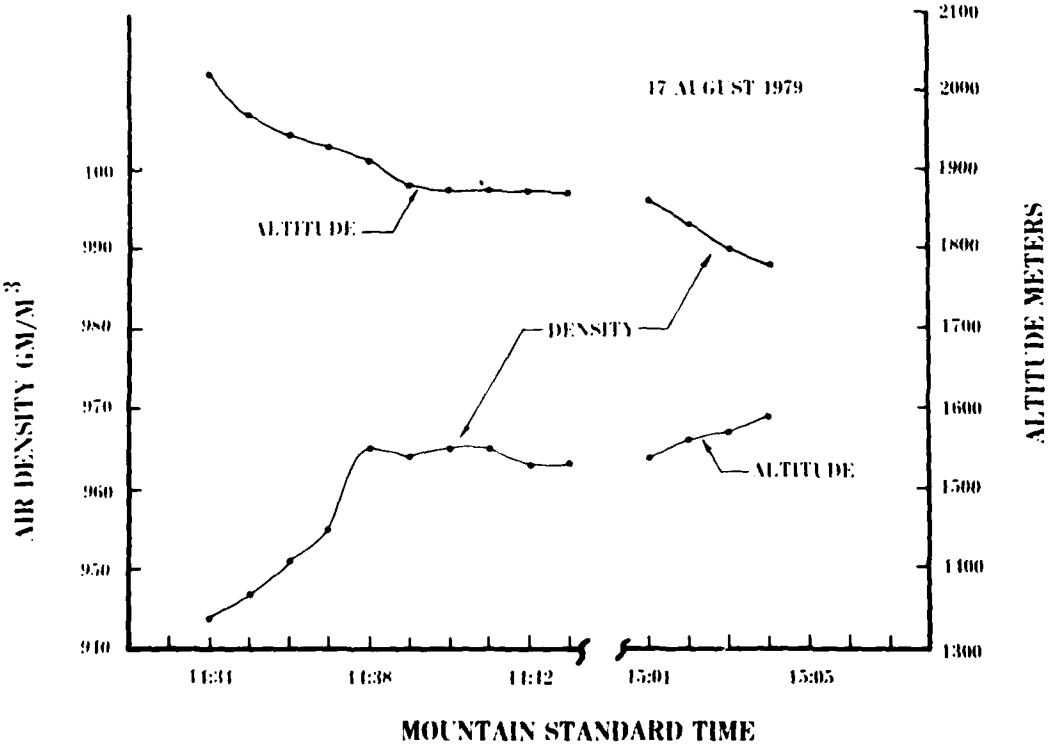

Figure 18. Air density as a function of time and altitude obtained with MAP aircraft.

were calm, and the sky was partly cloudy. It may be assumed that the aerosols collected aboard the MAP are representative of those in the atmsophere over the laser range under similar weather conditions.

As indicated previously in the discussion of the PIXE impactor, figure 9 shows the channel (mass) number spectrum of aerosols, 16μm or larger, collected by the impactor that was flown on the MAP on 17 August 1979. Corresponding to figure 9, the bar chart of figure 19 shows the total mass found in the sample as a function of atomic mass number. The zinc (Zn) is from the mylar/substrate disk of the impactor. The elements silicon (Si), sulfur (S), potassium (K), calcium (Ca), and iron (Fe) are constituents normally found in desert clays such as kalonite, montmorillonite, illite, and gypsum, which are typical at WSMR.[9] Chlorine (Cl) is also known to be a constituent of the local soil.[10] The sources of titanium (Ti), phosphorus (P), cobalt (Co), and vanadium (V) in the airborne impactor were not investigated.

Analysis of 16μm and larger aerosols that were simultaneously collected on the earth's surface at WSMR by another PIXE impactor showed approximately 10 percent greater mass per element than did the analysis of the aircraft-borne sampler disk. In addition, the analysis of the ground-based sampler showed traces of manganese, nickel, and lead. The manganese is believed to be from the limonite associated with limestone sediments at WSMR. The lead is suspected to come from the exhausts of vehicles commonly used at WSMR. The source of nickel was not established. These three elements were not present in the airborne impactor.

In addition to the requirements for atmospheric and aerosol data directly over the laser range, a requirement exists for aerosol and turbulence data along laser propagation paths in the proximity of a sheer cliff that is also located on WSMR. To satisfy this requirement, the instrumented MAP was employed to make a group of flights near the escarpment in directions generally transverse to the cliff wall.

Figure 20 shows the general terrain features, the location where the laser is housed, and the location of the airstrip (15 x 150 m) used by the MAP. The cliff summit is 2400 m msl, while the airstrip at the base of cliff is 1700 m msl. Horizontal flights directly away from and directly toward the cliff face were conducted at altitudes of 2130, 2440, 2740, 3047, 3350, and 3660 m, all altitudes referenced to msl.

The total payload weight aboard the MAP was 9 kg. Atmospheric temperature, pressure, and RH measurement were again made, with instrumentation identical to that used in previous flights. To derive turbulence structure data, measurements of differences in temperature, T, were made with sensor separations

---

[9]Blanco, J. A., and G. B. Hoidale, Infrared Absorption Spectra of Atmospheric Dust, ECOM-5193 (AD836883), Atmospheric Sciences Laboratory, US Army Electronics Command, White Sands Missile Range, NM, 1968.

[10]Soil Survey of White Sands Missile Range, NM, US Department of Agriculture Soil Conservation Service, January 1976.

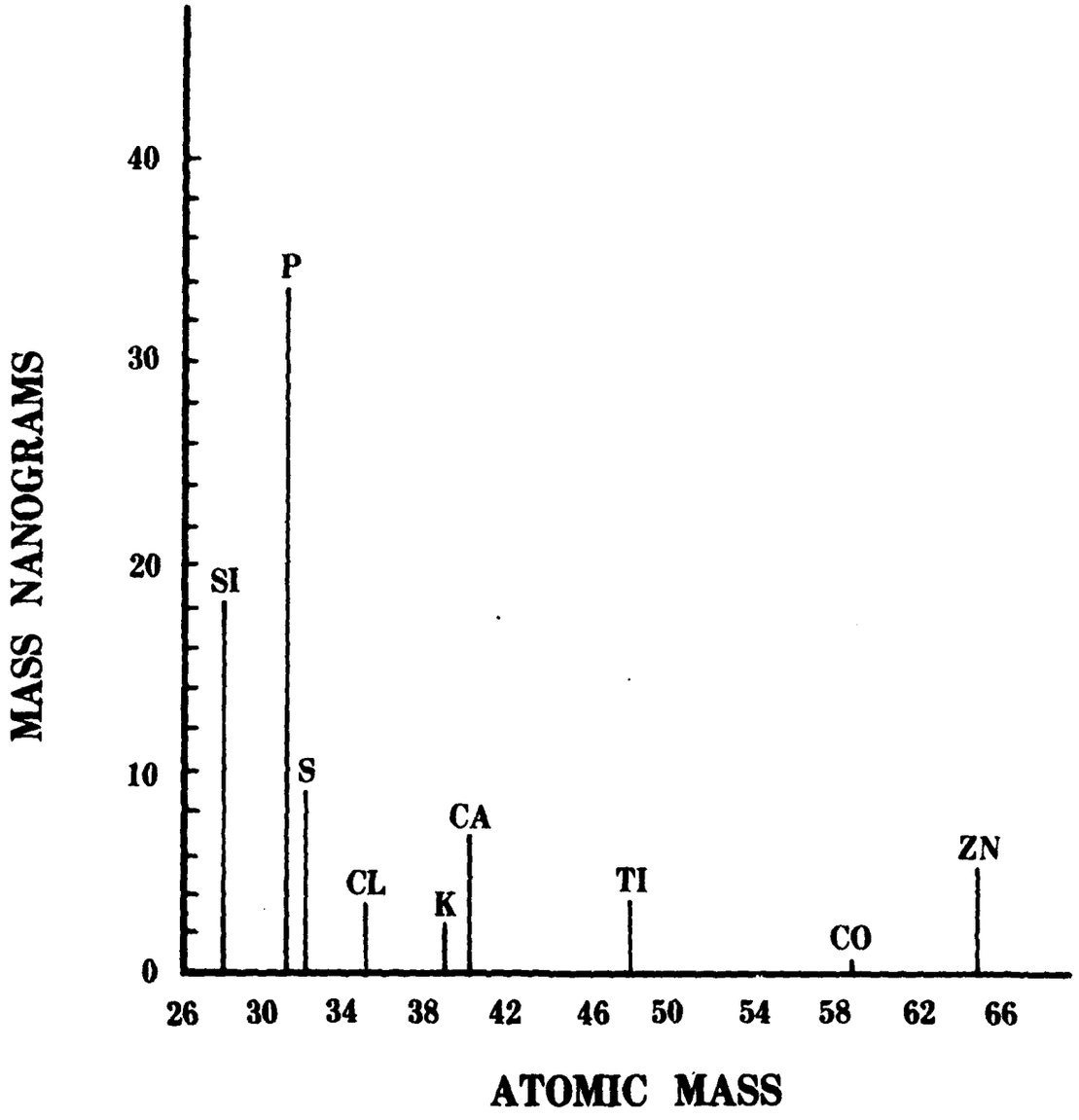

Figure 19. Total elemental mass found in the integrated aerosol sample of figure 9.

Figure 20. View of escarpment environment sampled with sensors on board the MAP aircraft.

of 20 cm and 2.8 m. The temperature difference values, when combined with the measured atmospheric temperature and pressure values, were used to determine C_T^2 and C_n^2 through equations (4) and (6), respectively.

Aerosol samples were collected with both the multistage sampler and the PIXE cascade impactor. Electric field intensity measurements were made as a function of altitude as the aircraft flew in close proximity to the cliff face, where the normal electric field gradients were affected by augmentation. The radar tracking of the VEGA transponder aboard the MAP by WSMR FPS/16 radars provided consistent and accurate position data for all of the flights conducted.

Unanticipated withdrawal of funds from the MAP project precluded an analysis of the aerosols collected by the two samplers; however, sufficient funds were obtained to reduce the atmospheric temperature, pressure, and RH measurements to meaningful data. Values of C_n^2 were calculated for all of the flights conducted, while electric field measurements were reduced to give the vertical potential gradient of the atmospheric electric field for the flight that was conducted on 10 July 1980.

Presented in this report are representative values of C_n^2, as well as values of the vertical potential gradient of the earth's electric field, which were obtained during the MAP flight of 10 July 1980. A more comprehensive and detailed report, which follows this one, will present atmospheric temperature, pressure, and RH data, as well as values of C_n^2 obtained during the MAP flights conducted on 27 June, and 2, 8, 9, and 10 July 1980.

Figure 21 is a graph of constant values of $\log_{10} C_n^2$ plotted as functions of altitude (msl) vs horizontal distance (km) to the laser site located on Oscura Peak at WSMR. These values were calculated from the data obtained from the various sensors aboard the MAP in the time interval 1200-1245 MST 9 July 1980. For the purpose of comparison, figure 22 presents similar C_n^2 data obtained from ground-based and balloon-borne sensors at WSMR in the time interval 0920-1000 MST 10 July 1980.

Figure 23 presents values of the vertical potential gradient of the earth's electric field as a function of altitude. These values were determined from the electric field sensors aboard the MAP during the flight of 10 July 1980.

Calibration of the electric field instrumentation was obtained by making low level aircraft passes over a ground-based electric field strength meter during a period when the surface electric field strength remained relatively constant at a value of 70 V/m. The data of figure 23 were extracted when the MAP aircraft was flying in level flight above the broad valley west of Oscura Peak at altitudes between 1685 and 3542 m. The corresponding horizontal distance from the mountain peak was approximately 2 km.

It has been observed that the vertical potential gradient of the earth's electric field usually decreases with increasing altitude; however, in the convection layer above desert terrain there are occasions when the gradient increases with increasing altitude. Figure 23 shows that this is the case here. On 10 July 1980, a day of high convective activity, the cloud bases were located at 3.8 km.

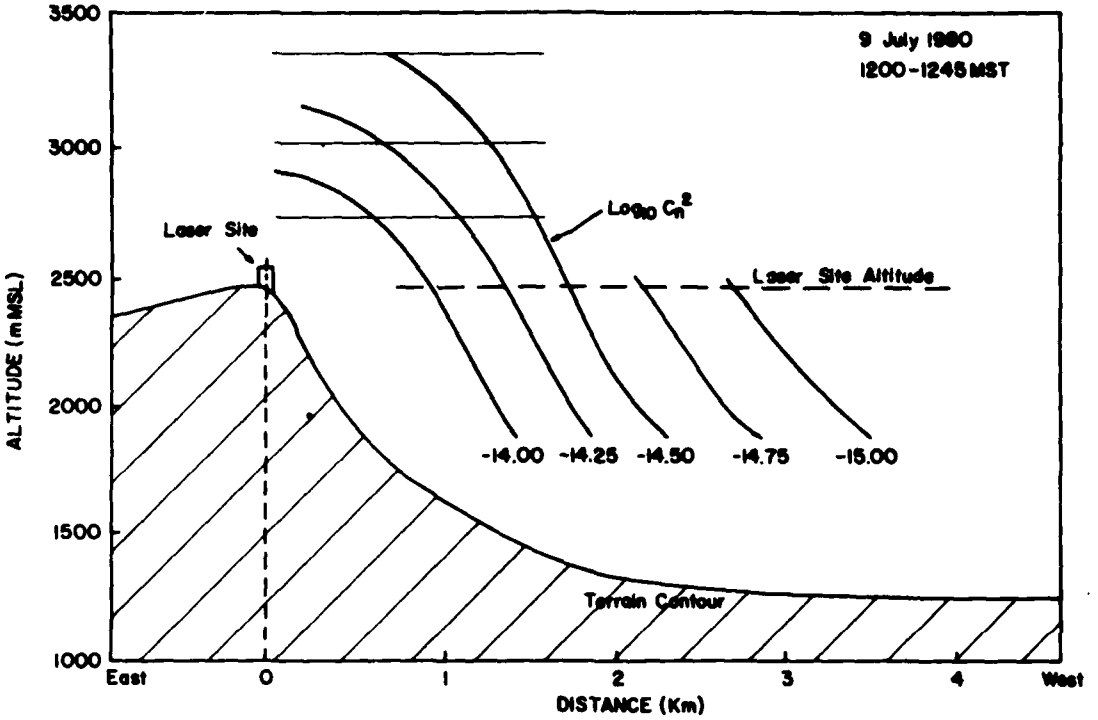

Figure 21. Constant values of $\log_{10} C_n^2$ as a function of altitude and horizontal distance from the laser site. These values were calculated from MAP sensor data recorded by North Oscura peak.

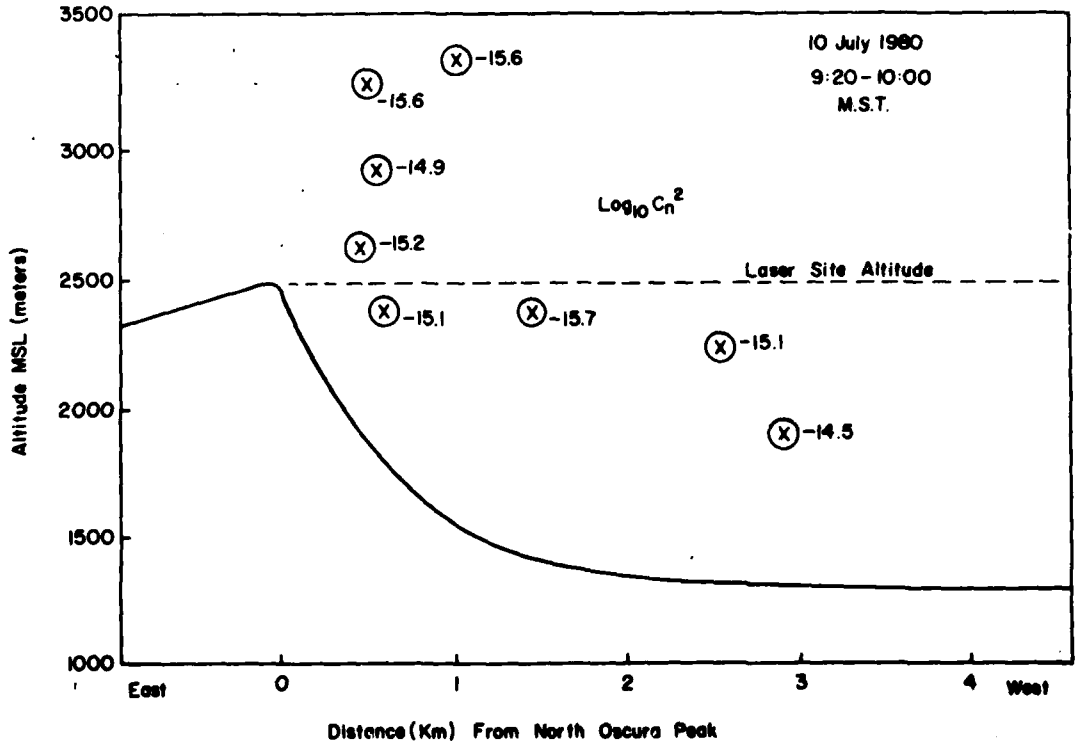

Figure 22. C_n^2 data obtained from ground-based and balloon-borne sensors by North Oscura Peak.

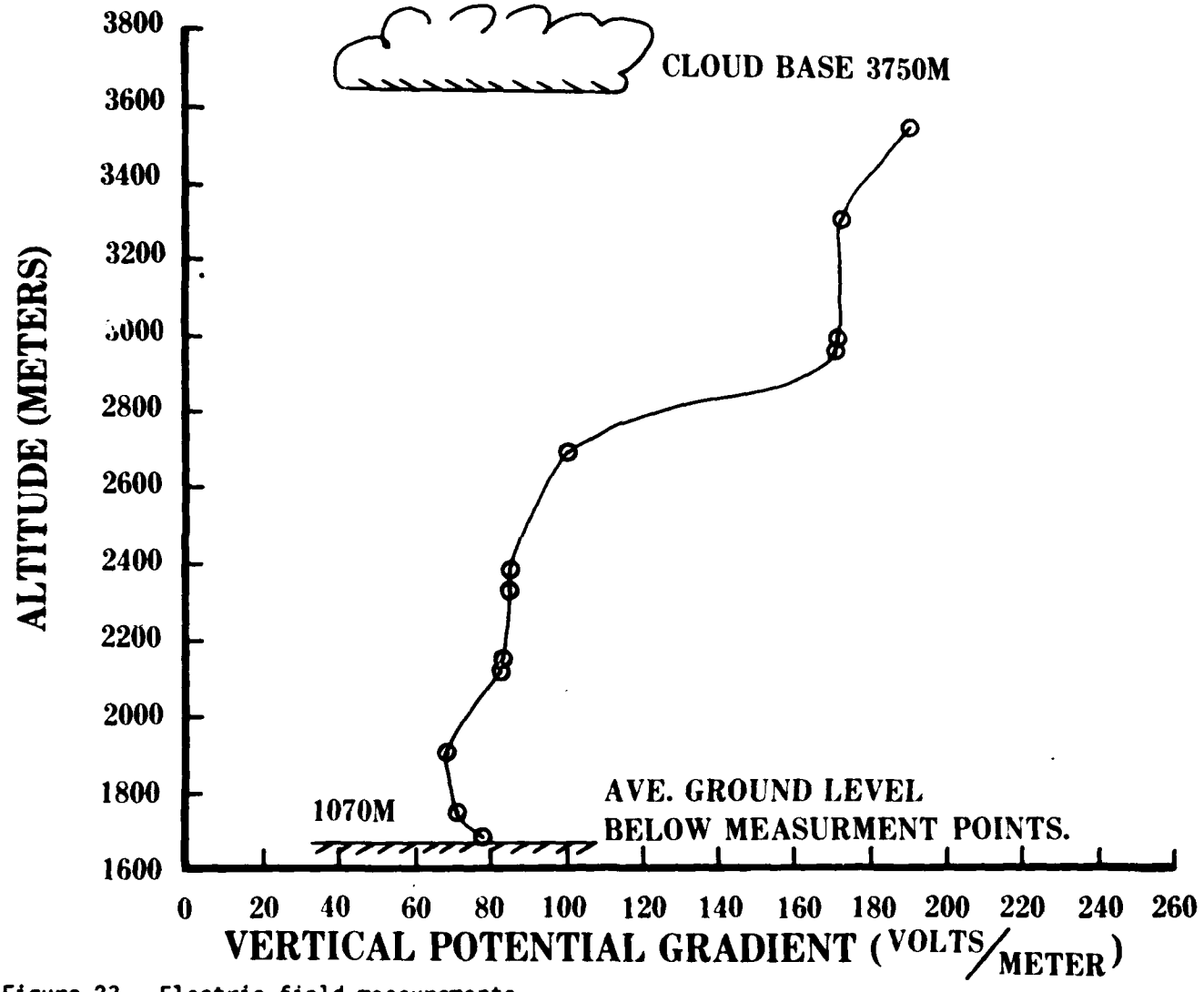

Figure 23. Electric field measurements.

These flights within the period 27 June to 10 July 1980 in the vicinity of the mountain peak also served to test the electrostatic and fluidic stabilizers aboard the MAP. Fair weather prevailed during all of the flights, and electrostatic stabilization relative to the earth's electric field was excellent.

Several tests were conducted wherein the aircraft, with the electrostatic autopilot engaged, was flown at the approximate height of Oscura peak on courses either perpendicular or parallel to the cliff face. Each time the MAP aircraft automatically turned and flew away from the cliff face when coming within approximately 200 m of it. These tests indicate that aircraft terrain avoidance can be accomplished through use of the electrostatic autopilot system.

Engagement of the fluidic stabilizer yielded adequate vertical stabilization, but indicated that fluidic stabilization is not as smooth and steady as electrostatic stabilization. Nevertheless, because of its all-weather capability to provide adequate stabilization at a low cost, the fluidic gyro will be used on future MAP aircraft.

SUMMARY

The program successfully accomplished its primary objectives of designing and fabricating a low-cost, yet reliable RPV and then instrumenting this RPV with meteorological sensors to demonstrate the feasibility of employing the aircraft to acquire atmospheric data in areas that are difficult or impossible to reach with conventional atmospheric sensor platforms.

Three groups of flights, as described in this report, clearly demonstrated the advantages of using an instrumented RPV to probe dust clouds, slant atmospheric paths along which laser beams propagate, and atmospheric regions in proximity to mountainous terrain. Flights with a payload weight of 11 kg to an altitude of 3660 m msl did not place undue stress on the MAP vehicle. Launchings and landings of this aircraft were readily accomplished from relatively flat areas 150 m in length and 15 m in width. Use of the small and inexpensive electrostatic autopilot and fluidic gyro stabilizer made aircraft control relatively simple.

Versatile aerodynamic and atmospheric sensors, with their associated electronic packages for signal conditioning and telemetry, were flight-tested and are now operational. Similarly, the associated MAP ground-based signal reception and data recording system is operational. This system is housed in a mobile van. The van is of sufficient size to also house two MAP aircraft with their associated launching and maintenance equipment, thus making the entire MAP system easily transportable to the specified test site.

Data presented in section 8 of this report demonstrate that sensors aboard the MAP can, with reasonable accuracy, measure the atmospheric parameters of temperature, pressure, RH (density-derived), turbulence structure constants, aerosol content, and earth's electric field intensity. Electron microscope analysis of the samples collected in dust clouds generated by artillery shell explosions gave information relative to particle sizes, particle size distribution, and elemental composition of the particles making up the dust cloud.

Determination of the collection efficiency of the impactor sampler, when combined with the recorded airspeed of the MAP, will yield aerosol concentration data.

Although not documented in this report, measurements of aircraft altitude, airspeed, engine revolution rate, heading, and angle of attack were recorded during each MAP flight.

In addition to the development of the MAP aircraft and its associated aerodynamic and atmospheric sensors, concurrent experimentation with the inexpensive electrostatic and fluidic gyro stabilizers has led to the basic units required to fabricate a low-cost autopilot suitable for a tactical RPV. Further refinements of the fluidic gyro are required to smooth its compensation commands. Further development of the electrostatic autopilot will likely lead to an inexpensive aircraft terrain-avoidance detector.

REFERENCES

1. Hill, M. L., "Introducing Electrostatic Autopilots," Astronautics and Aeronautics, November 1972.

2. Ballard, H. N., and R. Rubio, "Corrections to Observed Rocketsonde and Balloonsonde Temperatures," J Appl Meteorol, 7:5, 1968.

3. Design Review Agenda for Meteorological Sounding System Radiosonde Design, Space Data Corporation, 10 April 1978.

4. Manufacturer's brochure of Cascade Impactors, PIXE International Corporation, PO Box 2235, Tallahassee, FL 32304.

5. Nelson,J. W., Proton Scattering Analysis for Light Elements in Air Particulate Matter, Report EPA-600/2-78-213, Environment Sciences Research Laboratory, November 1978.

6. Maneuverable Atmospheric Probe/North Oscura Peak Experiment, Schellenger Research Laborabory Report FRI-80-UA-89, The University of Texas at El Paso, El Paso, TX, 1980.

7. Telemetry User's Handbook, Department of the Army, White Sands Missile Range, NM, 1 January 1977.

8. Kennedy, B. W., Dusty Infrared Test-II (DIRT-II) Program, ASL-TR-0058, US Army Atmospheric Sciences Laboratory, White Sands Missile Range, NM, 1980.

9. Blanco, J. A., and G. B. Hoidale, Infrared Absorption Spectra of Atmospheric Dust, ECOM-5193, AD836883, Atmospheric Sciences Laboratory, US Army Electronics Command, White Sands Missile Range, NM 1968.

10. Soil Survey of White Sands Missile Range, NM, US Department of Agriculture Soil Conservation Service, January 1976.

DISTRIBUTION LIST

Commander
US Army Aviation Center
ATTN: ATZQ-D-MA
Fort Rucker, AL 36362

John M. Hobbie
c/o Kentron International
2003 Byrd Spring Road
Huntsville, AL 35807

Chief, Atmospheric Sciences Div
Code ES-81
NASA
Marshall Space Flight Center, AL 35812

Commander
US Army Missile Command
ATTN: DRDMI-RRA/Dr. O. M. Essenwanger
Redstone Arselal, AL 35809

Commander
US Army Missile Command
ATTN: DRSMI-OG (B. W. Fowler)
Redstone Arsenal, AL 35809

Commander
US Army Missile R&D Command
ATTN: DRDMI-TEM (R. Haraway)
Redstone Arsenal, AL 35809

Redstone Scientific Information Center
ATTN: DRSMI-RPRD (Documents)
US Army Missile Command
Redstone Arsenal, AL 35809

Commander
HQ, Fort Huachuca
ATTN: Tech Ref Div
Fort Huachuca, AZ 85613

Commander
US Army Intelligence
Center & School
ATTN: ATSI-CD-MD
Fort Huachuca, AZ 85613

Commander
US Army Yuma Proving Ground
ATTN: Technical Library
Bldg 2105
Yuma, AZ 85364

Dr. Frank D. Eaton
Geophysical Institute
University of Alaska
Fairbanks, AK 99701

Naval Weapons Center
Code 3918
ATTN: Dr. A. Shlanta
China Lake, CA 93555

Commanding Officer
Naval Envir Prediction Rsch Facility
ATTN; Library
Monterey, CA 93940

Sylvania Elec Sys Western Div
ATTN: Technical Reports Lib
PO Box 205
Mountain View, CA 94040

Tetra Tech Inc.
ATTN: L. Baboolal
630 N. Rosemead Blvd.
Pasadena, CA 91107

Geophysics Officer
PMTC Code 3250
Pacific Missile Test Center
Point Mugu, CA 93042

Commander
Naval Ocean Systems Center
(Code 4473)
ATTN: Technical Library
San Diego, CA 92152

Meteorologist in Charge
Kwajalein Missile Range
PO Box 67
APO San Francisco, CA 96555

Director
NOAA/ERL/APCL R31
RB3-Room 567
Boulder, CO 80302

Library-R-51-Tech Reports
NOAA/ERL
320 S. Broadway
Boulder, CO 80303

National Center for Atmos Rsch
Mesa Library
P. O. Box 3000
Boulder, CO 80307

Dr. B. A. Silverman D-1200
Office of Atmos Resources Management
Water and Power Resources Service
PO Box 25007
Denver Federal Center, Bldg. 67
Denver, CO 80225

Hugh W. Albers (Executive Secretary)
CAO Subcommittee on Atmos Rsch
National Science Foundation Room 510
Washington, DC 2055

Dr. Eugene W. Bierly
Director, Division of Atmos Sciences
National Scinece Foundation
1800 G Street, N.W.
Washington, DC 20550

Commanding Officer
Naval Research Laboratory
Code 2627
Washington, DC 20375

Defense Communications Agency
Technical Library Center
Code 222
Washington, DC 20305

Director
Naval Research Laboratory
Code 5530
Washington, DC 20375

Dr. J. M. MacCallum
Naval Research Laboratory
Code 1409
Washington, DC 20375

HQDA (DAMI-ISP/H. Tax)
Washington, DC 20314

HQDA (DAEN-RDM/Dr. de Percin)
Washington, DC 20314

The Library of Congress
ATTN: Exchange & Gift Div
Washington, DC 20540
2

Mil Asst for Atmos Sci Ofc of
the Undersecretary of Defense
for Rsch & Engr/E&LS - RM 3D129
The Pentagon
Washington, DC 20301

Dr. John L. Walsh
Code 6534
Navy Research Lab
Washington,DC 20375

AFATL/DLODL
Technical Library
Eglin AFB, FL 32542

Naval Training Equipment Center
ATTN: Technical Information Center
Orlando, FL 32813

Technical Library
Chemical Systems Laboratory
Aberdeen Proving Ground, MD 21010

US Army Materiel Systems
Analysis Activity
ATTN: DRXSY-MP
APG, MD 21005

Commander
ERADCOM
ATTN: DRDEL-PA/ILS/-ED
2800 Powder Mill Road
Adelphi, MD 20783

Commander
ERADCOM
ATTN: DRDEL-PAO (M. Singleton)
2800 Powder Mill Road
Adelphi, MD 20783

Commander
ERADCOM
ATTN: DRDEL-ST-T (Dr. B. Zarwyn)
2800 Powder Mill Road
Adelphi, MD 20783
02

Commander
Harry Diamond Laboratories
ATTN: DELHD-CO
2800 Powder Mill Road
Adelphi, MD 20783

Chief
Intel Mat Dev & Spt Ofc
ATTN: DELEW-WL-I
Bldg 4554
Fort George G. Mead, MD 20755

Acquisitions Section, IRDB-D823
Library & Info Svc Div, NOAA
6009 Executive Blvd.
Rockville, MD 20752

Naval Surface Weapons Center
White Oak Library
Silver Spring, MD 20910

Air Force Geophysics Laboratory
ATTN: LCC (A. S. Carten, Jr.)
Hanscom AFB, MA 01731

Air Force Geophysics Laboratory
ATTN: LYD
Hanscom AFB, MA 01731

Meteorology Division
AFGL/LY
Hanscom AFB, MA 01731

The Environmental Research
Institute of MI
ATTN: IRIA Library
PO Box 8618
Ann Arbor, MI 48107

Mr. William A. Main
USDA Forest Service
1407 S. Harrison Road
East Lansing, MI 48823

Dr. A. D. Belmont
Research Division
PO Box 1249
Control Data Corp
Minneapolis, MN 55440

Commander
Naval Oceanography Command
Bay St. Louis, MS 39529

Commanding Officer
US Army Armament R&D Command
ATTN; DRDAR-TSS Bldg 59
Dover, NJ 07801

Commander
ERADCOM Scientific Advisor
ATTN: DRDEL-SA
Fort Monmouth, NJ 07703

Commander
ERADCOM Tech Support Activity
ATTN: DELSD-L
Fort Monmouth, NJ 07703

Commander
HQ, US Army Avionics R&D Actv
ATTN: DAVAA-O
Fort Monmouth, NJ 07703

Commander
USA Elect Warfare Lab
ATTN: DELEW-DA (File Cy)
Fort Monmouth, NJ 07703

Commander
US Army Electronics R&D Command
ATTN: DELCS-S
Fort Monmouth, NJ 07703

Commander
US Army Satellite Comm Agency
ATTN: DRCPM-SC-3
Fort Monmouth, NJ 07703

Commander/Director
US Army Combat Survl & Target
Acquisition Laboratory
ATTN: DELCS-D
Fort Monmouth, NJ 07703

Director
Night Vision & Electro-Optics Laboratory
ATTN: DELNV-L (Dr. R. Buser)
Fort Belvoir, VA 22060

Project Manager
FIREFINDER/REMBASS
ATTN: DRCPM-FFR-TM
Fort Monmouth, NJ 07703

6585 TG/WE
Holloman AFB, NM 88330

AFWL/Technical Library (SUL)
Kirtland AFB, NM 87117

AFWL/WE
Kirtland, AFB, NM 87117

TRASANA
ATTN: ATAA-SL (D. Anguiano)
WSMR, NM 88002

Commander
US Army White Sands Missile Range
ATTN: STEWS-PT-AL
White Sands Missile Range, NM 88002

Rome Air Development Center
ATTN: Documents Library
TSLD (Bette Smith)
Griffiss AFB, NY 13441

Environmental Protection Agency
Meteorology Laboratory, MD 80
Rsch Triangle Park, NC 27711

US Army Research Office
ATTN: DRXRO-PP
PO Box 12211
Rsch Triangle Park, NC 27709

Commandant
US Army Field Artillery School
ATTN: ATSF-CD-MS (Mr. Farmer)
Fort Sill, OK 73503

Commandant
US Army Field Artillery School
ATTN: ATSF-CF-R
Fort Sill, OK 73503

Commandant
US Army Field Artillery School
ATTN: Morris Swett Library
Fort Sill, OK 73503

Commander
US Army Dugway Proving Ground
ATTN: STEDP-MT-DA-M
(Mr. Paul Carlson)
Dugway, UT 84022

Commander
US Army Dugway Proving Ground
ATTN: MT-DA-L
Dugway, UT 84022

US Army Dugway Proving Ground
ATTN: STEDP-MT-DA-T
(Dr. W. A. Peterson)
Dugway, UT 84022

Inge Dirmhirn, Professor
Utah State University, UMC 48
Logan, UT 84322

Defense Technical Information Center
ATTN: DTIC-DDA-2
Cameron Station, Bldg. 5
Alexandria, VA 22314
12

Commanding Officer
US Army Foreign Sci & Tech Cen
ATTN: DRXST-IS1
220 7th Street, NE
Charlottesville, VA 22901

Naval Surface Weapons Center
Code G65
Dahlgren, VA 22448

Commander
US Army Night Vision
& Electro-Optics Lab
ATTN: DELNV-D
Fort Belvoir, VA 22060

Commander
USATRADOC
ATTN: ATCD-FA
Fort Monroe, VA 23651

Commander
USATRADOC
ATTN: ATCD-IR
Fort Monroe, VA 23651

Dept of the Air Force
5WW/DN
Langley AFB, VA 23665

US Army Nuclear & Cml Agency
ATTN: MONA-WE
Springfield, VA 22150

Director
US Army Signals Warfare Lab
ATTN: DELSW-OS (Dr. Burkhardt)
Vint Hill Farms Station
Warrenton, VA 22186

Commander
US Army Cold Regions Test Cen
ATTN: STECR-OP-PM
APO Seattle, WA 98733


DATE:
ILME